Mineralogical aspects of interstratified chlorite/smectite associated with epithermal ore veins: A case study of the Todoroki Au-Ag ore deposit, Japan

T. Yoneda[1], T. Watanabe [2] and T. Sato[3]

1: Hokkaido University, Sapporo, 060-8628, Japan, e-mail: yonet@eng.hokudai.ac.jp,

2: Niigata College of Nursing, Joetsu, 943-0147 Japan, 3: Faculty of Engineering,

Hokkaido University, Sapporo, 060-8628, Japan

ABSTRACT: Chlorite (C) − corrensite (Co) − smectite (S) series minerals occur as vein constituents in the two epithermal ore veins, the Chuetsu and Shuetsu veins of the Todoroki Au-Ag deposit. The occurrence characteristics of the C-Co-S series minerals indicate that the clays may be products of direct precipitation from hydrothermal fluids and subsequent mineralogical transformations during and/or after vein formation. The minerals from the Chuetsu vein are characterized by 'monomineralic' corrensite showing an extensive distribution throuhgout the vein, and tri-octahedral smectite occurring locally. The Shuetsu vein minerals are characterized by C-Co series minerals which can be divided into three different types: a I type including discrete chlorite with minor amounts of S layers, a II type comprising interstratified C/Co and discrete chlorite, and a III type characterized by segregation structures of C and Co layers. The types of C-Co series minerals show slightly different spatial distributions in the Shuetsu vein. Different epithermal environments during the vein formations and possible kinetic effects may have played a role in the formation and conversion of Co-C series at the Shuetsu vein and S-Co series at the Chuetsu vein.

KEYWORDS: chlorite-corrensite-smectite series minerals, interstratified chlorite/ corrensite mineral, epithermal Au-Ag ore vein, environmental conditions.

INTRODUCTION

It is well known that trioctahedral chlorite (C) − trioctahedral smectite (S) series minerals including corrensite (Co), a 1:1 regularly interstratified mineral of chlorite and smectite (or vermiculite) layers, occur extensively in different geological environments (Sudo & Shimoda, 1977; Velde, 1985; Beaufort et al., 1997; Meunier, 2003). Recent studies of minerals of this series from diagenetic, low-grade metamorphic, and hydrothermal environments show that corrensite mostly occurs as a stable single phase, and in many cases the series of minerals occur as a discontinuous sequence with steps of different interstratification of chlorite and smectite layers (e.g., Inoue & Utada, 1991; Shau & Peacor, 1992; Buatier et al., 1995; Beaufort et al., 1997; Fukui & Yoshimura, 1999; Drits et al., 2011; Kogure et al., 2013). In these cases chlorite-rich interstratified chlorite/smectite (C/S) mineral series have been dominantly observed and mostly described as mixtures of corrensite and chlorite, but corrensite mixed with interstratified C/S phase has also been reported (Leoni et al., 2010). However in some cases the corrensite-chlorite series is described as a continuous series of interstratifications of chlorite and smectite layers (Schiffman & Fridleiffson, 1991; Bettison-Varga & Mackinnon, 1997). The transformation mechanism and controlling factors implicated in the smectite to chlorite conversion series have been discussed in recent papers (Shau & Peacor, 1992; Beaufort et al., 1997; Robinson et al., 2002; Kogure et al., 2013). It is noteworthy that the transformation of smectite to chlorite in the case of hydrothermally altered basalts is related to fluid/rock ratios (Shau & Peacor,

1992). Moreover the mineral transformation in geothermal systems is controlled by kinetic effects linked to the fluid/rock ratios or modes of fluid transport (advection or diffusion) related to the rates of dissolution/nucleation/growth, in addition to temperatures as the primary factors in the transformation (Robinson et al., 2002).

It is also well known that mafic phyllosilicates commonly occur as vein minerals in hydrothermal metallic ore veins (Nagasawa et al., 1976; Shirozu, 1978), and especially interstratified C/S minerals are found as vein minerals in some epithermal Au-Ag ore veins (Taguchi & Watanabe, 1973; Yoneda & Watanabe, 1981, 1989, 1994; Takeuchi, 1984) (Fig. 1). However, detailed features of interstratified C/S minerals from epithermal Au-Ag ore veins have not been described like those in other geological environments.

In epithermal vein deposits the vein minerals are formed generally by precipitation from hydrothermal solution in open fractures. The fluid/rock ratio during formation of the vein minerals can be presumed to be much higher than that of the secondary minerals in wall rock. In addition, the ore forming processes in epithermal systems (boiling, cooling, oxidation, mixing, and others) may affect the mineralogical features of the C-S series minerals as well as the mineral assemblages and metal contents of the ore deposits (White & Hedenquist, 1990). A better knowledge of the mineralogical sequence of C/S minerals formed as vein constituents under epithermal conditions would help to understand the transformation mechanisms and factors controlling the mineral formation in such geological systems. Further, the relationship between the C/S mineral series in the ore veins and the Au-Ag mineralization would be useful indicators in the exploration of ore deposits. In this study the occurrence and the mineralogical properties of C/S minerals occurring as vein constituents from two epithermal Au-Ag ore veins (the Chuetsu vein and the Shuetsu vein) of the Todoroki

deposit are described based on observations of optical and scanning electron microscopy (SEM), X-ray powder diffraction analysis (XRD), XRD modeling of C/S interstratification, and chemical analyses by electron probe micro-analysis (EPMA) and analytical transmission electron microscopy (AEM). The mineralogical changes in minerals of the smectite to chlorite conversion series and their conditions of formation in the epithermal ore veins are discussed with respect to their phase relationships with the coexisting minerals.

ORE VEINS AND SAMPLES STUDIED

The Todoroki ore deposit is located in southwestern Hokkaido and is comprised of epitherma1 Au-Ag bearing quartz veins. The Chuetsu and Shuetsu veins, the principal ore veins, are situated at the western and eastern parts of the mining district respectively, and are hosted chiefly in rhyolitic pyroclastic rocks and sandstone/ mudstone with tuff of the middle Miocene age (Yoneda, 1994) (Fig. 2). A K-Ar dating for adularia and sericite in hydrothermally altered wall rocks of the Chuetsu and Shuetsu veins indicated respectively 2.09−3.05 Ma and 2.08 Ma, and these K-Ar ages show that the Au-Ag ore veins may be genetically related to the Pliocene volcanic activity which produced the andesite rocks found directly over the ore veins in this area (Sawai et al., 1992).

The scale of the veins of the mined parts of the Chuetsu and Shuetsu veins have approximate lengths of 600m along the strike and 140m along the dip with a mean thickness (mined part) of 3m, and 980m (strike), 120m (dip), and 4.5m (mean thickness of mined part), respectively (Japan Mining Industry Association, 1968). The sampling sites at the Shuetsu vein in this study were restricted to the deep central and eastern parts of the vein, because the major parts of the vein have been mined, and those at the Chuetsu vein were more spread out in the vein but not from the shallow high-grade

parts which have been mined.

The constituents of the Chuetsu and Shuetsu veins can be broadly divided into three different formation stages (Hasegawa et al., 1976; Yoneda, 1994). The earlier stage (I) is characterized by dark gray, massive quartz observable locally as small veins in the Chuetsu vein. In the middle stage (II), quartz occurs as the most common constituent of the two ore veins. Further the stage II quartz may be divided into different sub-stages such as white or gray massive quartz veins and white/grey banded quartz veins with or without rhodochrosite, as shown in Fig. 3. The massive and banded veins of the stage II are dominated by microcrystalline and fine-grained quartz, with occurrences of coarse-gained quartz or comb quartz band. Though a comprehensive chronological relationship among the quartz veins in the different sub-stages is difficult to elucidate, observations of the ore veins show that the white massive quartz vein is earlier than the other quartz veins, and that the quartz vein with rhodochrosite occurred in a later sub-stage. The stage II quartz veins are associated with Au-Ag minerals and Cu-Pb-Zn-Fe sulfide minerals in addition to clays as seen in Fig.4. The Au-Ag/Cu-Pb-Zn-Fe-S minerals are aggregated in the form of black streaks and patches in the stage II quartz, showing a close relationship to formations of clays as seen in some hand specimens of ore samples (Fig. 4). The later stage (III) is composed of calcite and quartz, and without Au-Ag/Cu-Pb-Zn-Fe minerals and clays.

The samples of this study were collected from vein quartz, wall rock including rock fragments trapped in the veins, and clay veins cutting through the ore veins or found between the ore veins and the wall rock as follows: stage I quartz (N=2), stage II quartz (N=81: 8 samples from 160 meters mine level (ml is used hereafter), 14 samples from 130ml, 13 samples from 110ml, 37 samples from 80ml and 9 samples from 50ml), wall rock (N=18), and veined clay (N=5) from the Chuetsu vein: stage II quartz

(N=43: 15 and 28 samples from the eastern part and the deep central part, respectively), wall rock (N=19), and veined clay (N=1) from the Shuetsu vein. Petrographic analyses were performed on the samples from the Chuetsu and Shuetsu veins (Yoneda, 1994).

The early stage samples from the Chuetsu vein are barren quartz with minor amounts of pyrite, adularia and clay minerals. Stage II quartz samples from the two ore veins are associated with minor amounts of Au-Ag minerals (electrum + argentite + pearceite ± polybasite + pyrargyrite ± argentian tetrahedrite) and small amounts of Cu-Pb-Zn-Fe sulfides (sphalerite + chalcopyrite + galena + pyrite ± marcasite) in the black streaks and patches. Clay minerals are also common constituents of stage II quartz samples as will be detailed below. Adularia is locally associated with the massive quartz of an early sub-stage in stage II quartz. In the later sub-stage samples of the stage II quartz, rhodochrosite + calcite assemblages are commonly found at the two ore veins.

The samples from the Shuetsu vein show higher Cu+Pb+Zn contents (7.49−0.28 wt%: N=9) than those from the Chuetsu vein (0.15−0.02 wt%: N=7). In addition, the chemical compositions of electrum and sphalerite in the ore samples show differences between the two ore veins: the Ag contents of electrum (0.62−0.54 atomic ratio, N=24, mean value = 0.58, SD = 0.027) and FeS contents of sphalerite (0.96−0.12 mol%, N = 113, mean value = 0.45, SD = 0.151) from the Shuetsu vein are higher than the Ag contents of electrum (0.52−0.43 atomic ratio, N = 19, mean value = 0.49, SD = 0.016) and FeS contents of sphalerite (0.16−0.01 mol%, N = 31, mean value = 0.04, SD = 0.03) from the Chuetsu vein.

The mineral assemblage of the wall rock samples is quartz + K-feldspar ± calcite + chlorite + illite ± pyrite at the Chuetsu vein, and quartz ± K-feldspar ± calcite + chlorite

± illite ± pyrite at the Shuetsu vein. Interstratified C/S minerals were rarely detected in the wall rock samples of the two mineralized epithermal veins. Illite ± kaolinite ± illite/smectite interstratified mineral were detected in the two veins.

METHODS

The clay minerals contained in the ore samples were extracted by hand-picking and separated by ultrasonic treatment in distilled water, and then the clay fractions were concentrated by centrifugal sedimentation as follows: rotation speed 1000r.p.m., distance from axis to surface of the suspension liquid 4.5cm, distance from axis to surface of settling particles 15.5cm, time 60sec, and the concentration taking place at room temperature. Samples of clay fractions, untreated (UT) and solvated by 10% ethylene glycol solution (EG), were mounted on glass slides to prepare oriented-specimens, and the oriented-specimens were examined by XRD using a Rigaku Geigerflex D-6C (radiation: Ni-filtered CuKα; accelerating voltage/current: 30 kV/10~20 mA; slit systems: divergent 1/6° -scattering 0.3 mm-receiving 1/6° or 1/2° -0.3mm-1/2° ; scan speed: 1 deg/min). In addition selected samples of clay fractions, saturated in KCl solution (K^+) and solvated by glycerol vapor after Mg saturation by $MgCl_2$ solution (MgGly), were prepared similarly to the oriented-specimens. XRD was performed by a Rigaku RU-300 with a graphite monochromator under the conditions of CuKα radiation, accelerating voltage/current: 40kV/200mA; slit systems: divergent 1/6° -scattering 0.3mm-receiving 1/6° or 1/2° -0.3mm-1/2° and step conditions: size 0.01 degree and counting time 1sec.

XRD peak deconvolution was performed to explore overlapping peaks from discrete phases, by using “Traces V5” (Diffraction Technology Pty. Ltd. Australia). XRD patterns of C/S interstratifications were modelized using a program coded by

Watanabe (1977, 1988), which calculates one dimensional X-ray line profiles based on Kakinoki & Komura (1952), and compared with the observed patterns.

AEM analysis were performed on clay particles deposited on copper mesh (150-mesh) covered by collodion foil, and then carbon coated after drying. The clay specimens were analyzed by a Hitachi H-700 equipped with an EDX analytical attachment (Horiba EMAX-2200) under the conditions of an accelerating voltage of 200 kV and an X-ray counting time of 100 sec or 200 sec.

Selected ore samples were prepared as polished thin sections for optical microscopic observations and EPMA analyses of clay minerals. The EPMA analyses were performed by a JXA-50A under the conditions of an accelerating voltage of 15 kV, specimen current of 0.01 μA, beam diameter of 10 μm, and counting time of 10sec. Standard samples used are quartz, rutile, synthetic Al_2O_3, synthetic $MnO\text{-}Fe_2O_3$ (1:1), synthetic MgO, wollastonite, synthetic Na-Ca glass, and adularia. Quantitative corrections were performed after Bence & Albee (1968). In addition chips from the selected ore samples were coated by Au and provided for SEM observations of the clay minerals using a JSM25S (accelerating voltage of 15kV).

RESULTS AND DISCUSSION

Petrography

Clays are closely associated with the stage II quartz veins basically showing crustiform quartz texture which is characterized by successive, narrow, subparallel layers of minerals precipitated successively (e.g. Shimizu, 2014) (Fig.4). Banded clay aggregates observed in the stage II quartz are concordant with the crustiform quartz

texture (Fig. 4A−C), and patched clay aggregates contained in the ore samples may be also concordant with the crustiform quartz texture, slightly deviated from typical one, where the clay aggregates are accompanied with similar patched aggregates of Au-Ag/Cu-Pb-Zn-Fe minerals in the same thick band of quartz (Fig. 4D).

Optical microscopic observations show that clay minerals occur as irregularly patched or finely banded aggregates of particles closely associated with quartz, ore minerals and locally with carbonates (Fig. 5). Clay minerals from the Chuetsu vein are generally composed of very fine-grained particles (Fig.5A) with coarse-grained particles (Fig.5B: tri-smectite). It is noteworthy that band aggregates have apparent concavo-convex surfaces in microcrystalline quartz (Fig.5A). This type of aggregate may be interpreted as a colloform texture of which form is retained even after re-crystallization to fine-grained clay particles. Clay minerals from the Shuetsu vein occur as similar aggregates (Fig. 5C, D) with coarser grained-particles (Fig. 5E). In addition, clay minerals observed in the black streaks and patches of the ore samples show evidence of simultaneous formation with sphalerite (Fig. 5D) and electrum-argentite (Fig. 5F).

Macroscopic and microscopic observations of clays/clay minerals mentioned above suggest that they may be products of direct precipitation from hydrothermal fluids in the middle stage of vein formation, and that initial precipitates from the hydrothermal fluids may have been amorphous materials based on the colloform texture that is generally interpreted to originate from gel deposition (e.g., Shimizu, 2014). The latter may be supported by the presence of amorphous materials precipitating as clay scales in geothermal wells (e.g., Reyes & Cardile, 1989). In addition, the microscopic occurrences suggest that the initial clay precipitates could be precursors which would be changed to fine-grained and/or coarser-grained clay particles in subsequent

dissolution/re-crystallization process.

The dominant clay minerals in the ore samples from the two veins are C/S mixed-layer minerals. These C/S minerals show differences in XRD basal reflections as illustrated in Fig. 6A, where XRD patterns of UT and EG specimens of the selected ore samples (C1, S1, S2, and S3) are shown. Accordingly, the C/S minerals can be distinguished into four types of mineralogical association (named I to IV type hereafter). It must be noted that the I−III types occur in the ore samples from the Shuetsu vein, whereas the IV type occur only in the ore samples from the Chuetsu vein. Optical microscopic images of the I-IV types are shown in Fig 5 (A: IV type, C: III type, D: II type and E: I type).

The I and II types show XRD basal reflections of chlorite, however the II type is also characterized by weak reflections at 30Å and 20Å which respectively shift to 31Å and 21Å, and by change in peak profile of the reflections at about 7.2 Å and 4.7 Å by EG treatment, (Fig. 6A). Some samples grouped into the I type show also slight changes in peak profile of the basal reflections after the EG treatment as seen in Fig. 6A. The reflections with a superstructure reflection at about 29Å (UT) observed in the types III and IV agree with to those of corrensite, however the III type shows significant changes in the shape of the higher order basal reflections after the EG treatment. Additionally, the tri-octahedral smectite is observed locally in the ore samples from the Chuetsu vein. The tri-octahedral smectite (d (060) = ~1.53Å) shows basal reflections with d-values deviating somewhat from those of typical saponite to vermiculite (Fig. 6B). In many cases the smectite can be observed as ‘monomineralic phase’ in the ore samples. Di-octahedral smectite coexisting with quartz and Mn oxides has been only reported in an ore sample from the upper oxidized zone (160ml) of the Chuetsu vein (Yoneda & Watanabe, 1981).

The IV type is distributed widely but the tri-smectite is of relatively limited distribution in the Chuetsu vein. This may be attributed to the temporal difference of clay formations: smectite may be associated with later sub-stage quartz, while the IV type is associated with earlier and major sub-stages in the vein formation. In the Shuetsu vein, the I type is dominantly distributed in the eastern part while the II and III types are dominant in the deep central part of the vein, but their temporal relationships between the I−III types are not clear. In some hand specimens with crustiform texture, different types of C/S minerals are observed separately in different clay bands of a hand specimen, but the banded clays show no specific trend of formation sequences for the I−III types. These characteristics in distribution of the clay minerals in each vein may be related to the hydrothermal environmental conditions and mineralogical conversion for the clay minerals which will be discussed later, in addition to the geological conditions (e.g., distributions of open spaces for mineral deposition and pathways for upwelling hydrothermal fluid).

The SEM observations were performed for selected samples of the I−IV types and smectite. The IV type of fine-grained and irregularly-curved particles (Fig. 7A) shows a different morphology from tri-smectite with coarser particles gathering like flower petals (Fig. 7B). The III type appears to be composed roughly of lathe-shaped particles less curved than the IV type (Fig. 7C). The II type is characterized by bundle-like aggregates of elongated particles (Fig. 7D), which may correspond to aggregates of the acicular or reed shaped particles observed in the optical microscopic observations of the II type. Other particles with different appearances are not distinctly recognized in the SEM observations of the II and III types. In the I type there are platy or flaky particles with slight curvatures (Fig. 7E).

In addition to the above, trace amounts of illite minerals including interstratified

illite/smectite and kaolin minerals are found mixed in the C/S minerals in the ore samples of the two veins. Illite minerals or kaolin mineral are also detected in infillings of druses of the ore samples. These minerals can be interpreted to result from a later event which post-dated the middle stage of the vein formation.

XRD characterization and C/S modeling

The parameters in calculating XRD patterns for C/S interstratifications are described as follows. A normal distribution function is incorporated in the program, and the calculation was performed with $\bar{N}$ (the mean number of layers) = 10 and σ=2.0 in this study. The calculated line profiles are comparable to the profiles obtained using the slit system (1/2° -0.3mm-1/2°) of the RAD-II diffractometer (RIGAKU Co. Ltd. Japan) (Watanabe, 1988). The atomic parameters of the fundamental layers used in the calculations for the XRD patterns are shown in Table 1. The tetrahedral and octahedral compositions used in the fundamental layers are comparable to those obtained by EPMA analysis for the I−IV types. The probability parameters for the calculations of the XRD patterns for the C/S interstratified structures including completely segregated structures (i.e. mixtures of two discrete phases), are shown in Fig. 8.

The Ⅳ type C/S mineral (sample: C1) has a superstructure reflection (UT: 29Å, EG: 31Å, K^+: 27Å, MgGly: 32.5Å), sub-order basal reflections at rational positions, and d (060) spacing at 1.543Å. The basal reflection after the MgGly-treatment shows that the expandable layer of the IV type mineral may be smectitic and not vermiculitic. The coefficients of variability (CV) for the proportionality of the higher-order reflections (CV_{EG}=0.22 for 10 reflections, CV_K=0.33 for 8 reflections, CV_{MgGly}=0.34 for 11 reflections) are <0.75 (Bailey, 1982), indicating that the IV type may be identified as corrensite. The observed XRD pattern of the EG-specimen (C1) shows

that corrensite occurs as a pure mineral phase in the clay fractions of the sample, containing minute amounts of kaolinite as impurities (Fig. 9A). The IV type can be characterized as a 'monomineralic phase' in the ore samples. The calculated XRD pattern of EG-corrensite (Fig. 9B), shows a slight difference in intensity ratios of peaks possibly due to the difference of Mg contents.

XRD patterns of the I type of C/S minerals deviate from that of a true chlorite structure by a broadening of peaks corresponding to basal reflections and the occurrence of a reflection due to a superstructure after EG-treatment (Fig. 10). These changes can be due to minor amounts of swelling layers interstratified with the chlorite layers. The I type can be grouped as a tri-octahedral chlorite with occasional smectite layers and a ratio in the chlorite structure which may be presumed to be <10%.

The XRD pattern of the II type is characterized by weak 30Å- and 20Å-reflections which shift respectively to 31Å and 21Å after the EG-treatment. After K^+ saturation, the XRD pattern of the II type shows peaks at 11Å, 9.3Å, and 7.7Å in addition to broadened peaks of the basal reflections corresponding to chlorite at 14.2Å, 7Å, 4.7Å, 3.55Å, and 2.84Å (Fig. 11A). Such XRD pattern is similar to that due to the C/S interstratification of the chlorite mineral occurring in the hydrothermal alteration zone of the Wanibuchi deposit, a Kuroko-type ore deposit in Japan (Watanabe et al., 1974). The XRD pattern of the II type can be explained as interstratifications of chlorite and corrensite layers (Yoneda & Watanabe, 1994).

Calculations of XRD patterns of the II type were performed for three different models of interstratified structures: 1) interstratifications (Reichweite g=3) of chlorite and tri-smectite, 2) interstratifications (Reichweite g=2) of chlorite and corrensite, and 3) interstratifications (Reichweite g=1) of chlorite (double layers) and corrensite. As a

result the structural model of the interstratifications (g=1) of chlorite (double layers) (0.7) and corrensite (0.3) with the probability point corresponding to 8 in Fig. 8 explains the characteristic XRD peaks of the II type. In this study this type of interstratified chlorite/corrensite is abbreviated as CC/Co. In addition the observed peaks corresponding to those of chlorite indicate that the II types can be interpreted as a mixture of the interstratified CC/Co mineral and discrete chlorite. A superimposed pattern (Fig. 11B d) of the calculated interstratified CC/Co (Fig. 11B b) onto chlorite (Fig. 11B c) fits the observed pattern of the II type (Fig. 11B a), and provides an approximate ratio of chlorite (0.5) and CC/Co (0.5) in the II type sample. Peak deconvolution of the same observed pattern was performed by non-linear least squares fitting using the Pseudo-Voigt profile function, after subtraction of a background by cubic curve fitting. Deconvolution with 7 and 3 elementary peaks respectively observed within $2\theta^{\circ}$ = 5−15 and $2\theta^{\circ}$ = 23−27 are shown in Fig. 12, suggesting that the overlapping peaks of the II type can be interpreted clearly to be resulting from a mixture of interstratified CC (0.7)/Co (0.3) mineral and discrete chlorite possibly having a low crystal-thickness distribution and/or randomly interstratified structure with small amounts of smectite.

The XRD pattern of the III type is characterized by changes in the basal reflections at 2θ=10°−28°, where the peak profiles at about 7−8Å, 4.4−5.2Å and 3.4−3.6Å changed after EG-treatment (Fig. 13A). A comparison of the XRD patterns with simulated patterns shows that the EG-S3 can be better understood as a segregation structure of chlorite (0.5) and corrensite (0.5) (Fig. 13A-c) rather than a mixture of the two discrete phases (Fig. 13A-b). The XRD patterns of K^{+} and MgGly-S3 are similar to the C/Co segregation structure. Other EG-samples of the III type, showing somewhat different variations of peak profiles at about 7−8Å, 4.4−5.2Å and 3.4−3.6Å, can be interpreted

to result from a C/Co segregation structure between C(0.3)/Co(0.7) and C(0.7)/Co(0.3), though the observed peak at about 2θ=25−26° of the sample #S80511B shows a larger segregation tendency as compared with others (Fig. 13B). Interstratified chlorite/saponite minerals showing a XRD pattern similar to the III type has previously been documented in the Kuroko ore deposits (Shirozu et al., 1975).

Chemical compositions of the chlorite-corrensite-smectite series minerals

Quantitative point analyses by EPMA of the interstratified C/Co minerals from 18 ore samples, tri-octahedral smectite from 2 ore samples, and tri-octahedral chlorite from 4 wall rock samples in contact with the ore veins, were performed and 321 analytical data-sets were obtained (Yoneda & Watanabe, 1989; Yoneda, 1994). For each selected samples, the analytical values in oxide wt% and in atomic% were averaged (Table 2).

The chlorite-corrensite-smectite (C-S) series minerals from the ore veins are Mg-rich and Fe-poor ones with small amounts of manganese, and show compositional features related to the types of C-S minerals and distinct differences from wall-rock chlorite. From the tri-octahedral smectite to IV type, III type, II type, I type and wall-rock chlorite, the Al/Si ratios, the tetrahedral negative-charges and the octahedral charges increase, while the interlayer charges decrease from IV type, III type, II type, I type and to wall-rock chlorite. These compositional variations relating to the types of C-S minerals can be understood to be due to the proportions of smectite layers comprising the various samples. In addition, the octahedral compositions of the C-S series minerals show a characteristic differences related to the types of C-S minerals as shown in the Mg-Fe-Al (VI) plots (Fig. 14). It is discriminative that the IV type and tri-smectite are very poor in Fe but abundantly rich in Mg as compared with the I−III types which are less Mg and more Fe. The wall-rock chlorites are poorer in Mg and

richer in Fe as compared to the I–III types. These differences in the octahedral compositions especially in Mg and Fe contents of the vein minerals can be explained by the compositions of hydrothermal fluids: Mg-rich & Fe-poor fluids in the Chuetsu vein and comparatively Mg-poor & Fe-rich fluids in the Shuetsu vein, based on the relationships between the precipitated clay compositions and the fluid compositions in geothermal wells (Reyes & Cardile, 1989).

An AEM analysis of the particles of C/S minerals from 11 ore samples has also been performed (Yoneda, 1994). EDX analyses were performed on both particles showing single-crystal and poly-crystal patterns in selected-area electron diffraction. Analytical results are represented in averaged structural formulae (Table 3). Compared with the EPMA analyses of the same samples, the standard deviations of each averaged values are large, and the values of Si and Na are high but Mg is low, suggesting that the analytical values may be affected by contamination in AEM analyses of this study. Averaged Al/Si ratios obtained by AEM and EPMA analyses are plotted together in Fig. 15. Despite a slight overestimation of Si content in the AEM analyses, the averaged Al/Si ratio obtained by EPMA and AEM analyses can be considered comparable. This would suggest that the variations in the Al/Si ratios observed in C-Co series minerals may arise due to differences within the scales of the clay particles, and that the discrete assemblage of chlorite and CC/Co of the II type and the assemblage showing a segregated structure of chlorite and corrensite of the III type can be understood to be packets incorporated in the stacking of clay particles.

Mineralogical changes and environmental conditions of formation

The I type mineral is chlorite with occasional smectite layers (10% ≥). The percentage of smectite layers (S%) in the II type (C + CC(0.7)/Co(0.3)) varies in a

limited range below 15% with a maximum value in absence of discrete chlorite. In the III type (C+Co) the smectite% can be estimated by using the XRD modeling of the C/S interstratifications as described above. The III type has a S% range of between 35%−15% and that of the IV type, monomineralic corrensite, can be estimated near 50%. Considering the percentage of smectite layers and the compositional variations of the chlorite-corrensite-smectite series minerals, the mineralogical differences in this mineral series in the two ore veins can be summarized as in Fig. 16. The Chuetsu and Shuetsu veins are characterized by different mineral series within the C-Co-S series minerals: a smectite-corrensite series at the Chuetsu vein and a corrensite-chlorite series at the Shuetsu vein. It is noteworthy that the former (Chuetsu) series of minerals (Fe/(Fe+Mg+Mn) = 0.01−0.03) shows much lower Fe contents than that of the Shuetsu series of minerals (Fe/(Fe+Mg+Mn) = 0.06−0.15), and that an interstratified phase of CC/Co is observed as a discrete phase in the C-Co series.

The interstratified C/S minerals being closely associated with Au-Ag and sulfide minerals in the ore samples which formed during the middle stage mineralization of the Chuetsu and Shuetsu veins, their conditions of formation can be approach from the condition of stability of the ore minerals.

The equilibrium temperature and S_2 fugacity of the electrum-sphalerite-pyrite-argentite assemblage may be expressed as a function of FeS% in sphalerite and the Ag mole ratio in electrum as the following sulfidation reactions (Barton & Toulmin, 1964, 1966; Vaughan & Craig, 1997).

$$2\,(FeS)_{sphalerite} + S_2 = 2\,FeS_2(pyrite) + H_2O \qquad (1)$$

$$4(Ag)_{electrum} + S_2 = 2Ag_2S(argentite) \qquad (2)$$

The intersection of two equilibrium curves of (1) and (2) here gives an invariant point of temperature and S_2 fugacity for an electrum-sphalerite-pyrite-argentite assemblage. If equilibrium is assumed during ore formation in each vein-type deposit, the compositions of sphalerite and electrum may permit to approximate temperature (electrum-sphalerite temperature) and S_2 fugacity (Shikazono, 1985). (140−242°C and 171−256°C for the Chuetsu and Shuetsu veins respectively). Based on the electrum-shpalerite-pyrite-argentite assemblages it may be suggested that ore deposition took place at higher temperature (171 to 256°C) in the Shuetsu vein than the Chuetsu vein (140 to 242°C), but at similar values of S_2 fugacity (log f_{S2} = −12.9 +0.05/−0.76 for the Chuetsu vein and log f_{S2} = −12.7 +0.29/−0.31 for the Shuetsu vein). Moreover, homogenization temperatures of primary and pseudo-secondary fluid inclusions of quartz from the middle stage ores of the two veins range from 140 to 270°C for the Chuetsu vein, and from 172 to 225°C for the Shuetsu vein (Yoneda, 1994).

In addition, the oxidation-reduction state of sulfur-containing aqueous solution co-existing with sphalerite and pyrite can be expressed as in the following reactions (Shikazono, 2003).

$$(FeS)_{sphalerite} + H_2S + 0.5O_2 = FeS_2\ (pyrite) + H_2O \qquad (3)$$

$$(FeS)_{sphalerite} + SO_4^{2-} + 2H^+ = FeS_2\ (pyrite) + H_2O + 1.5O_2 \qquad (4)$$

Equation (3) is for a reduced sulfur predominant region, and equation (4) is for an oxidized sulfur predominant region. Accordingly, the FeS content of sphalerite may be linked to the physicochemical conditions of the hydrothermal solution such as temperature, concentration of dissolved sulfur species, pH, and oxygen fugacity (Barnes & Kullerud, 1961). The possible ranges of pH and oxygen fugacity for the mineral assemblage of pyrite + sphalerite − kaolinite ± potassium mica ± adularia −

kaolinite − barite were calculated at a temperature of 200°C, a total potassium concentration of 10^{-1} mol/kg H_2O and a total sulfur concentration of 10^{-3} mol/kg H_2O, by using the thermodynamic data of Helgeson (1969), Helgeson & Kirkham (1974) and Helgeson et al. (1978), and the maximum/minimum FeS contents of sphalerite in the two veins. On the basis of the thermodynamic stability of the mineral assemblage mentioned above, the physicochemical parameters of pH and oxygen fugacity indicate that the hydrothermal environments of the II stage ore formations in the two veins could be in the reduced sulfur species predominant conditions and in pH conditions around neutral, but with different redox conditions between the Chuetsu and Shuetsu veins: the calculated log f_{O_2} (atm) ranges of −38 ~ −40 presumable for the Chuetsu vein and of −40 ~ −42 presumable for the Shuetsu vein show a higher oxidation state in the Chuestu vein. This tendency of the redox conditions in the reduced sulfur predominant region is the same at other temperatures close to 200°C, because the oxygen fugacity of the mineral assemblage depends on the FeS contents of the sphalerite included in the assemblage.

On the basis of the occurrences of chlorite-corrensite-smectite series minerals, it is possible that the minerals may have been formed by precipitation from upwelling hydrothermal fluids, which may have reacted with rocks in the deeper strata, during the middle stage of the epithermal systems. If the periods and water/rock ratios of the vein formation can be assumed to be similar in the Chuetsu and Shuetsu veins, it may be inferred that the difference in the electrum-sphalerite formation temperatures and/or in chemical compositions of the hydrothermal fluids may have played a role in the formation of the Co-C series at the Shuetsu vein and of the S-Co series at the Chuetsu vein. Additionally difference in redox conditions of the ore formation could have affected the crystal chemistry of the smectite-corrensite-chlorite series minerals.

Further investigations will be necessary to verify such hypothesis. Moreover, hydrothermal events such as boiling, mixing and cooling of upwelling fluids, which have large influences on the hydrothermal condition for mineral deposition in the epithermal systems (e.g., White & Hedenquist, 1990; Lonker et al., 1993), could be a factor to affect the formation of S-Co and Co-C series minerals. Especially the variation of boiling conditions, of which intensity may be linked to the formation of banded quartz with the crustiform, colloform, microcrystalline and comb textures in epithermal veins (Shimizu, 2014), may be likely to influence on the middle stage mineral formation in the Chuetsu and Shuetsu ore veins.

The formations of S-Co and Co-C series in the two ore veins can be attributed to the difference of temperatures and/or chemical composition of solutions invilved in the formation process of the two epithermal veins. In addition the spatial and/or temporal mineralogical changes of trioctahedral clay minerals can be a product of a transformation process including dissolution, re-precipitation, and crystal growth similar to that described in both diagenetic or hydrothermal environments (Beaufort et al., 2015 and references therein) during and subsequent to the vein formation. These kinetic effects may have implicated in the mineralogical conversion for the S → Co series at the Chuetsu vein and for Co → C series at the Shuetsu vein in addition to the predominant hydrothermal conditions during the vein formation mentioned above.

A chronology for the formation of clay minerals in two ore veins may be considered as follows. In the Chuetsu vein, Mg-rich & Fe-poor amorphous materials (precursor) may have been precipitated from hydrothermal fluids through the middle stage of ore formation, and consecutively transformed to smectitic materials and then to corrensite. However at later sub-stage of the middle stage, the smectitic materials

may have been grown to well-crystallized tri-smectite possibly in a lower temperature as compared with the temperature that the conversion to corrensite was dominated. On the other hand, comparatively Mg-poor & Fe-rich amorphous materials (precursor) may have been precipitated from hydrothermal fluids through the middle stage of ore formation, and consecutively transformed to corrensitic materials and then to chlorite in the Shuetsu vein. Though the transformation of precursor to corrensitic materials is uncertainty, the higher temperatures during ore formation in the Shuetsu vein may have influenced the mineralogical conversion which is different from that in the Chuetsu vein. In addition, the spatial and temporal variations in the occurrence of the I−III type minerals may be understood that the transformation of the Co → C had been affected by the variation of environmental conditions possibly due to the hydrothermal events occurred in the epithermal systems.

CONCLUSIONS

Chlorite-corrensite-smectite series minerals occur as vein constituents in the two epithermal Au-Ag ore veins, the Chuetsu vein and the Shuetsu vein of the Todoroki Au-Ag ore deposit. The occurrence characteristics of the minerals indicate that the clay minerals may be products of direct precipitation from hydrothermal fluids and subsequent mineralogical changes during and after vein formation. The series of minerals from the Chuetsu vein are characterized by ‘monomineralic’ corrensite showing an extensive disribution througout the vein, and tri-octahedral smectite occuring locally. The occurrence of smectite may be due to a product of relatively later sub-stages of the vein formation as compared with corrensite. The Shuetsu vein series minerals are characterized by chlorite/smectite minerals which can be divided into

three different types: I type including chlorite with minor amounts of smectite layers, II type comprising chlorite/corrensite mixed-layers and discrete chlorite, and III type characterized by segregation of corrensite and chlorite layers.

Based on the occurrences of the series of minerals and the chemistry of the co-existing minerals in the ore samples, the differences in the temperature and/or compositions of the hydrothermal fluids may be related to the formation of the IV type and tri-smectite at the Chuetsu vein, and of the I−III types at the Shuetsu vein. Finally the difference and variation of the epithermal environments during the vein formations and possible kinetic effects may have played a role in both the formation of corrensite, then its conversion to chlorite in the Shuetsu vein and the formation of smectite, then its conversion to corrensite in the Chuetsu vein.

Acknowledgments The authors wish to express their gratitude to Dr. D. Beaufort and two anonymous referees for their valuable comments and advice on an earlier version of the manuscript, and to Professor Torkil Christensen for his English corrections to the manuscript.

REFERENCES

Barnes H. L. & Kullerud G. (1961) Equilibria in sulfur-containing aqueous solutions in the system Fe-S-O, and their correlation during ore deposition. *Economic Geology*, **56**, 648-685.

Barton P. B. Jr. & Toulmin P. (1964) The electrum-tarnish method for the determination of fugacity of sulfur in laboratory sulfide systems. *Geochimica et Cosmochimica Acta*, **28**, 619-640.

Barton P. B. Jr. & Toulmin P. (1966) Phase relations involving sphalerite in Fe-Zn-S system. *Economic geology*, **61**, 815-849.

Beaufort D., Baronnet A., Lanson B. & Meunier A. (1997) Corrensite: A single phse or

a mixed-layer phyllosilicate in the saponite-to-chlorite conversion series? A case study of Sancerre-Couy deep drill hole (France). *American Mineralogist*, **82,** 109-124.

Beaufort D., Rigault C., Billon S., Billault V., Inoue, A. Inoue S., and Patrier P. (2015) Chlorite and chloritization processes through mixed layer mineral series in low-temperature geological systems - A review. *Clay Minerals*, **50**, 497-523.

Bence A.E. & Albee, A.L. (1968) Empirical correction factors for the electron microanalysis of silicates and oxides. *The Journal of Geology*, **76**, 382-403.

Bettison-Varga L. & Mackinnon I.D.R. (1997) The role of randomly mixed-layered chlorite/smectite in the transformation of smectite to chlorite. *Clays and Clay Minerals*, **45**, 506-516.

Buatier M. D., Früh-Green G. L. & Karpoff A. M. (1995) Mechanisms of Mg-phyllosilicate formation in a sedimented ridge (Middle Valley, Juan de Fuca). *Contribution of Mineralogy and Petrology*, **122**, 134-151.

Drits V.A., Ivanovskaya T.A., Sakharov B.A., Zviagina B.B., Gor'kova N.V., Pokrovskaya E.V. & Savichev A.T. (2011) Mixed-layer corrensite—chloites and their formation mechanism in the glauconitic sandstone — clayey rocks (Riphean, AnabaruUplift), *Lithology and Mineral Resources*, **46**, 566-593.

Fukui M. & Yoshimura T. (1999) Chlorite/Smectite mixed-layer minerals in Aosawa basalts distributed in the Dewa hill, Yamagata Prefecture. *Journal of the Clay Science Society of Japan*, **39**, 19-36 (in Japanese with English abstract).

Hasegawa K., Mitani K., Sugimoto R., Futamae K. & Hayakawa F. (1976) Geology and ore deposits of the Todoroki and Meiji district in Shikaribetsu province, Hokkaido. *Reports of Geological Survey of Hokkaido*, **48**, 33-60 (in Japanese with English abstract).

Helgeson H. C. (1969) Thermodynamics of hydrothermal systems at elevated temperatures and pressures. *American Journal of Science*, **267**, 729-804.

Helgeson H.C. & Kirkham D.H. (1974): Theoretical prediction of the thermodynamic behavior of aqueous electrolytes at high pressures and temperatures. I. Summary of

the thermodynamic/electrostatic properties of the solvent. *American Journal of Science*, **274**, 1089-1198.

Helgeson H. C., Delany J. M., Nesbitt H.W. & Bird D. K. (1978) Summary and critique of the thermodynamic properties of rock-forming minerals. *American Journal of Science*, **278-A**, 1－229.

Inoue A. & Utada M. (1991) Smectite-to-chlorite transformation in thermally metamorphosed volcanoclastic rocks in the Kamikita area, northern Honshu, Japan. *American Mineralogist*, **76**, 628-640.

Japan Mining Industry Association (1968) Todoroki mine. Pp. 2150-153 in: *List of Ore deposits of Japan*. Japan Mining Industry Association, Tokyo, Japan (in Japanese).

Kakinoki J. & Komura Y. (1952) Intensity of X-ray by an one-dimensionally disordered crystal. *Journal of Physical Society of Japan*, **7**, 30-35.

Kogure T., Drits V.A. & Inoue S. (2013) Structure of mixed-layer corrensite-chlorite revealed by high-resolution transmission electron microcopy (HRTEM). *American Mineralogist*, **98**, 1253-1260.

Leoni L., Lezzerini M., Battaglia S. & Cavalcante F. (2010) Corrensite and chlorite-rich Chl-S mixed layers in sandstones from the `Macigno' Formation (northwestern Tuscany, Italy). *Clay Minerals*, **45**, 87-106.

Lonker S.W., Franzson, H. & Kristmannsdottir, H. (1993) Mineral-fluid interaction in the Reykjanes and Svartsengi geothermal systems, Iceland. *American Journal of Science*, **293**, 605-670.

Meunier A. (2003) Clays, pp. 329-415. Springer, Berlin.

Nagasawa K., Shirozu H. & Nakamura T. (1976) Clay minerals as constituents of hydrothermal metallic vein-type deposits. *Mining Geology Special Issue*, **7**, 75-84 (in Japanese with English abstract).

Reyes, A.G. & Cardile C.M. (1989) Characterization of clay scales forming in Philippine geothermal wells. *Geothermics*, **18**, 429-446.

Reynolds, R.C. (1980) Interstratified clay minerals, Pp. 249-303 in: Crystal structures of clay minerals and their X-ray identification (G.W. Brindley & G. Brown, editor),

Min. Soc., London.

Robinson D., Schmidt S.T. & Santana de Zamora A. (2002) Reaction pathways and reaction progress for the smectite-to-chlorite transformation: evidence from hydrothermally altered metabasites. *Metamorphic Geology*, **20**, 167-174.

Sato, M. (1965) Structure of interstratified (mixed-layer) minerals. *Nature*, **208**, 70-71.

Sato, M. (1987) Interstratified (mixed layer) structures and their theoretical X-ray powder patterns I. theoretical aspects. *Clay Science*, **7**, 41-48.

Sawai O., Yoneda T. & Itaya T. (1992) K-Ar ages of the Chitose, Todoroki and Teine Au-Ag vein-type deposits, Southwest Hokkaido, Japan. *Mining Geology*, **42**, 323-330 (in Japanese with English abstract).

Schiffman P. & Fridleiffson, G.O. (1991) The smectite to chlorite transition in drillhole NJ-15, Hesjavellir geothermalfield, Iceland: XRD, BSE and electron microprobe investigations. *Journal of Metamorphic Geology*, **9**, 679-696.

Shau Y.H. & Peacor D.R. (1992) Phyllosilicates in hydrothermally altered basalts from DSDP Hole 504B, Leg 83 — a TEM and AEM study. *Contributions to Mineralogy and Petrology*, **112**, 119-133.

Shikazono N. (2003) Geochemical and tectonic evolution of arc-backarc hydrothermal systems.pp. 83-201. Elsevier, Amsterdam.

Shimizu T. (2014) Reinterpretation of quartz textures in terms of hydrothermal fluid evolution at the Koryu Au-Ag deposit, Japan. *Economic Geology*, **109,** 2051-2065

Shirozu H., Sakasegawa T., Katsumoto N. & Ozaki M. (1975) Mg-chlorite and interstratified Mg-chlorite/saponite associated with kuroko deposits. *Clay Science*, **4**, 305-321.

Shirozu H. (1978) Chlorite minerals. Pp. 243-264 in: *Clays and Clay Minerals of Japan* (T. Sudo & S. Shimoda, editors). Developments in Sedimentology 26, Elsevier, US.

Sudo T. & Shimoda S. (1977) Interstratified clay minerals − mode of occurrence and origin. *Minerals Science and Engineering*, **9**, 3-24.

Takeuchi K. (1984) Clay minerals in Arakawa No.4 vein of the Kushikino mine. *Mining Geology*, **34**, 335-342 (in Japanese with English abstract).

Taguchi S. & Watanabe T. (1973) Clay minerals especially interstratified chlorite/saponite associated with gold ores of the Fuke mine, Kagoshima prefecture. *Science Reports, Department of geology, Kyushu University*, **11**, 243-250 (in Japanese with English abstract).

Vaughan D. J. & Craig J. R. (1997) Sulfide ore mineral stabilities, morphologies, and intergrowth textures. Pp. 367-434 in: Geochemistry of hydrothermal ore deposits Third edition (H. L. Barnes, editor), John Wiley & Sons, Inc., New York.

Velde B. (1985) Clay minerals, pp.104-191. Elsevier, Amsterdam.

Watanabe T., Nakamuta Y. & Shirozu H. (1974) An interstratified mineral of chlorite and saponite from the Wanibuchi mine. *Journal of the Mineralogical Society of Japan,* **11,** Special Issue No.1, 123-130 (in Japanese with English abstract).

Watanabe T. (1977) X-ray line profile of interstratified chlorite/saponite. *Science Reports, Department of geology, Kyushu University*, **12**, 303-309 (in Japanese with English abstract).

Watanabe T. (1988) The structural model of illite/smectite interstratified mineral and the diagram for its identification. *Clay Science*, **7**, 97-117.

White N. C. & Hedenquist J. W. (1990) Epithremal environments and styles of mineralization: variations and their causes, and guideline for exploration. *Journal of Geochemical Exploration*, **36**, 445-474.

Yoneda T. & Watanabe T. (1981) Clay minerals in the gold-silver ore of the Chuetsu-hi vein of the Todoroki mine, Hokkaido, Japan. *Mining geology Special Issue*, **10**, 143-149 (in Japanese with English abstract).

Yoneda T. & Watanabe T. (1989) Chemical composition of regularly interstratified chlorite/smectite in the ores from some Neogene gold-silver vein-type deposits in Japan. *Mining geology*, **39**, 181-190 (in Japanese with English abstract).

Yoneda T. (1994) *Applied mineralogical study of clays from hydrothermal ore deposits*.

PhD thesis, Kyushu University, Japan (in Japanese).

Yoneda T. & Watanabe T. (1994) Chlorite/smectite mixed-layer mineral having a 20 A-reflection from the Todoroki epithermal gold-silver ore-vein. *Journal of Clay Scocity of Japan*, **34**, 71-79 (in Japanese with English abstract).

FIGURES

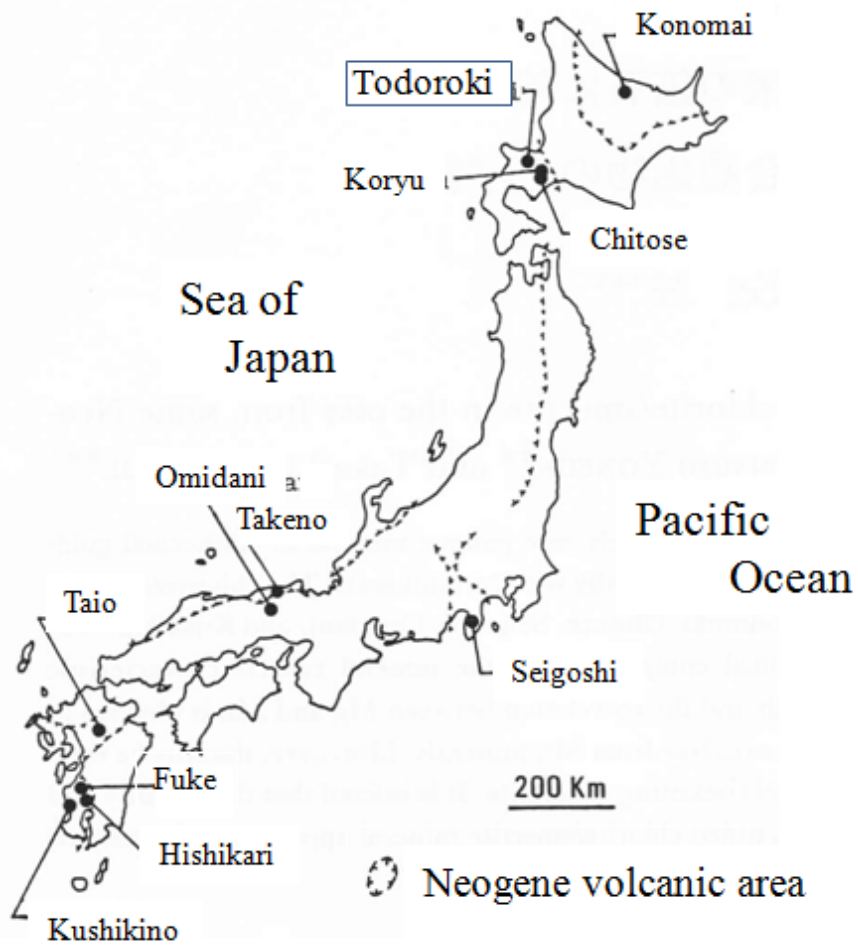

Fig. 1 Epithermal Au-Ag vein-type ore deposits where productions of interstratified C/S minerals have been described as vein minerals (Taguchi & Watanabe, 1973; Yoneda & Watanabe, 1981; Takeuchi, 1984; Yoneda & Watanabe, 1989).

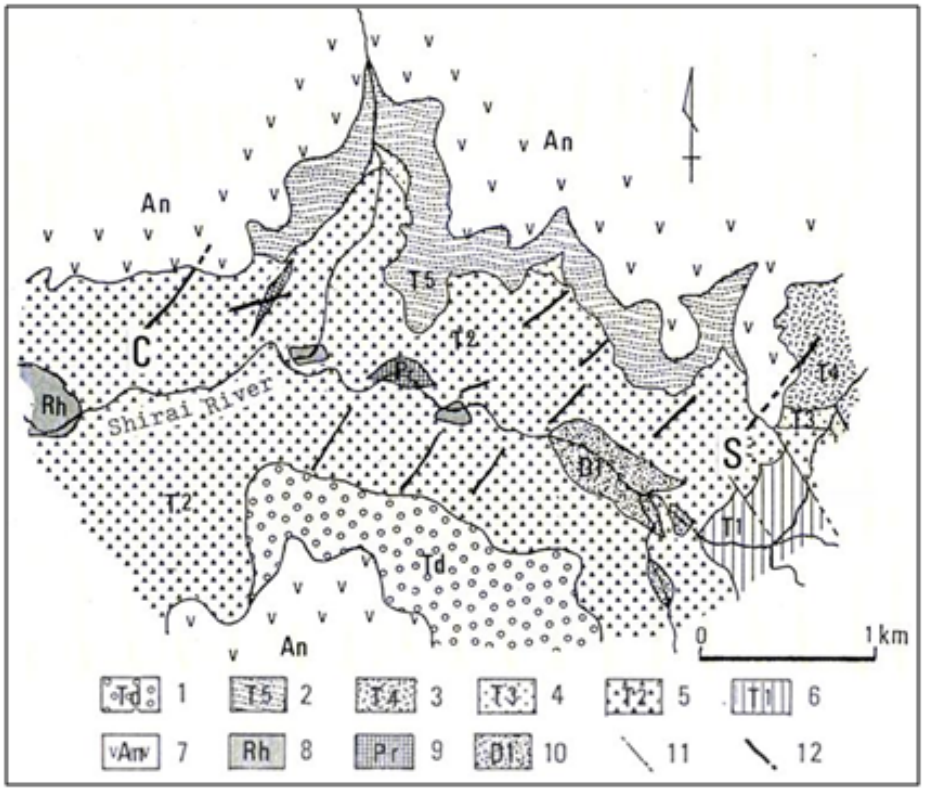

Fig. 2 Geological map of the Todoroki Au-Ag ore deposits (Hasegawa et al., 1976; Yoneda, 1994).

1: Talus deposit, 2: Tuff/sandstone with coal seam, 3: Andesitic tuff, 4: Sandstone/mudstone, 5: Rhyolitic tuff and tuff breccia, 6: Conglomerate/ mudstone/tuff, 7: Andesite lava, 8: Rhyolite, 9: Propylite, 10: Dolerite, 11: Fault, 12: Ore veins (C: Chuetsu vein, S: Shuetsu vein)

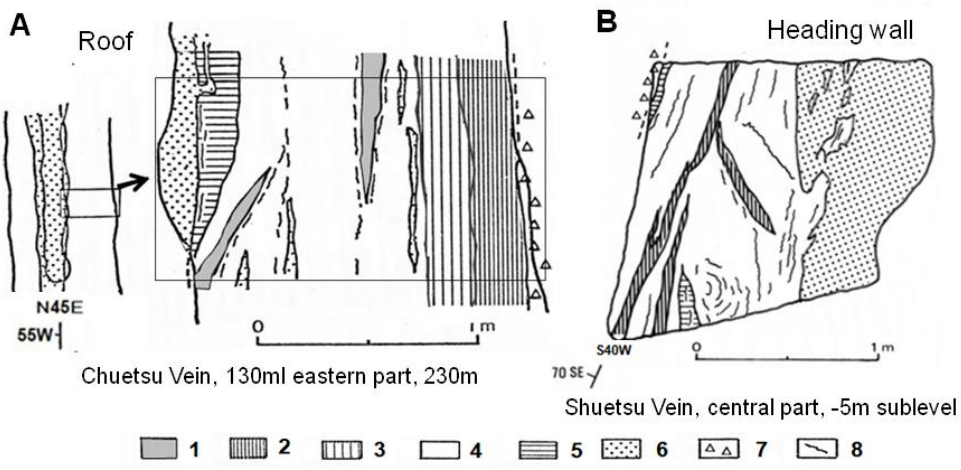

Fig. 3 Vein sketches showing the constituents and structures of the Chuetsu and Shuetsu veins. See in the text for details.

1: dark gray massive quartz (the I stage), 2: white/gray banded quartz with Au-Ag minerals/Cu-Pb-Zn-Fe-S sulfides (the II stage), 3: white/gray banded quartz with rhodochrosite and Au-Ag minerals/Cu-Pb-Zn-Fe sulfide minerals (the II stage), 4: gray quartz (partly banded) (the II stage), 5: white massive quartz (the II stage), 6: calcite (the III stage), 7: wall rock, 8: black streak rich in Au-Ag minerals/Cu-Pb-Zn-Fe sulfide minerals (AgB).

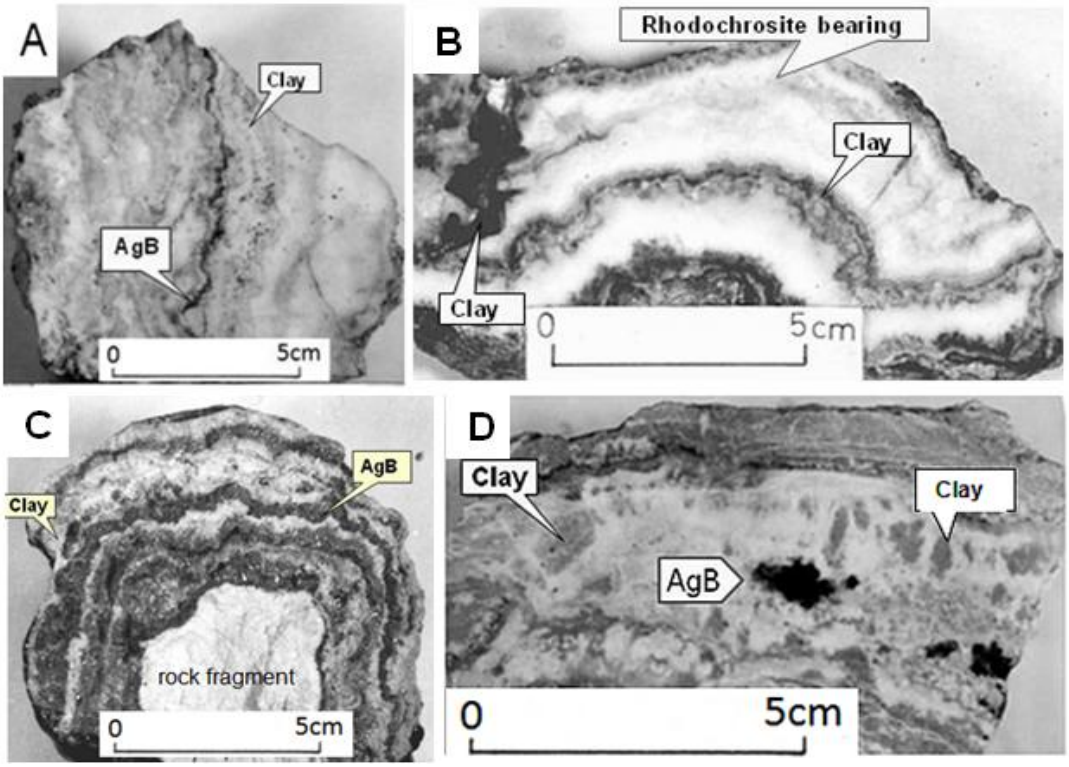

Fig. 4 Ore samples with ore minerals and clays from the middle stage quartz veins.

A: Banded quartz with Au-Ag minerals/Cu-Pb-Zn-Fe sulfide minerals (AgB) and clays (Chuetsau 130ml, #C80304), B: Banded quartz with rhodochrosite and clays (Chuetsau 50ml, #C71408), C: Banded quartz with AgB rich in Cu-Pb-Zn sulfides and clays crusting a rock fragment (Shuetsu central lower part, #S80509), D: quartz with patchy AgB and patchy ~ banded clays (Shuetsu eastern part, #S80601).

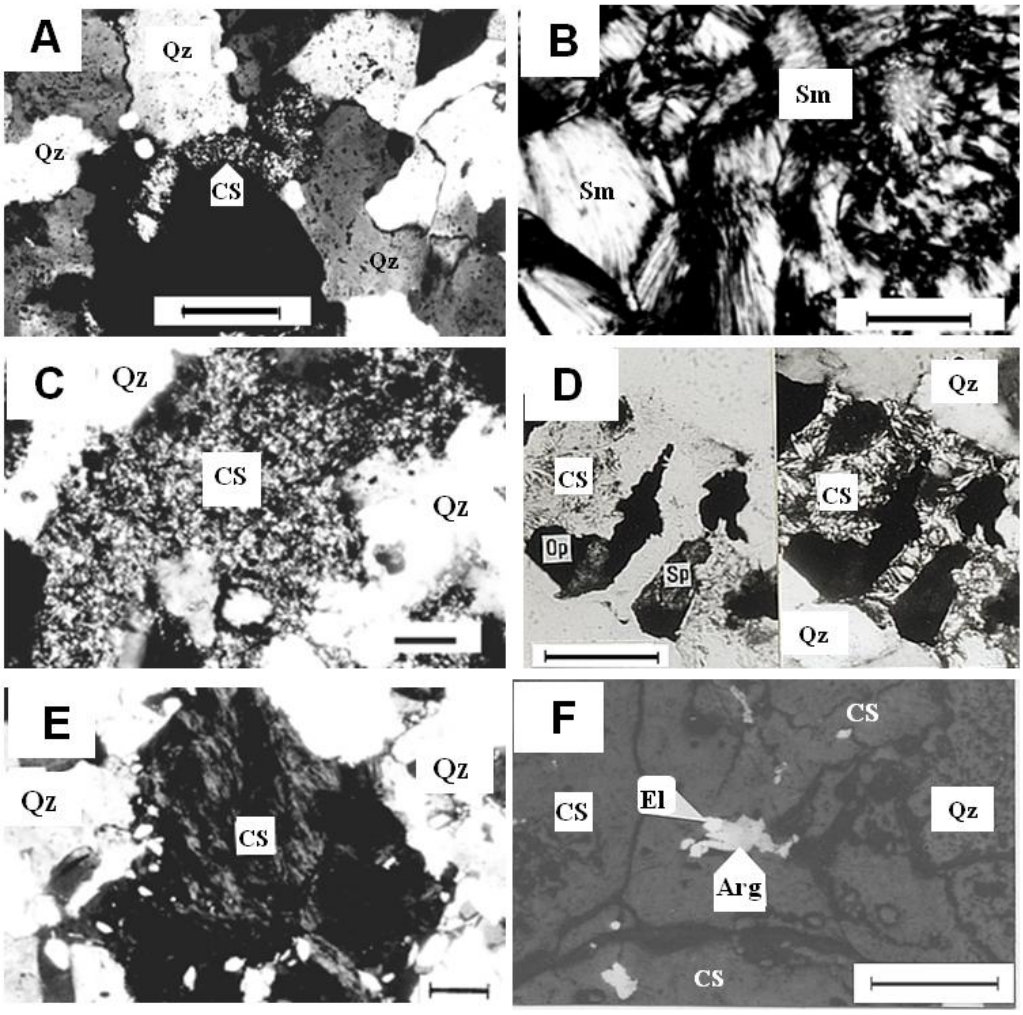

Fig. 5 Microphotographs of the clay minerals observed in the ore samples. A-C & E: transmitted light (cross polar), D: transmitted light (left half-parallel, right half-cross), F: reflected light (parallel polar). Bar scale: 100μm, Qz: quartz, CS: chlorite-smectite series mineral, Sm: smectite, Op: opaque ore mineral, Sp: sphalerite, El: electrum, Arg: argentite.

A: C1 (#C50507) − IV type, B: C10 (#C80304) − tri-smectite, C: #S80508C − III type, D: #S80508A − II type, E: #S80607 − I type, F: #C11204 − IV type. See in the text for details.

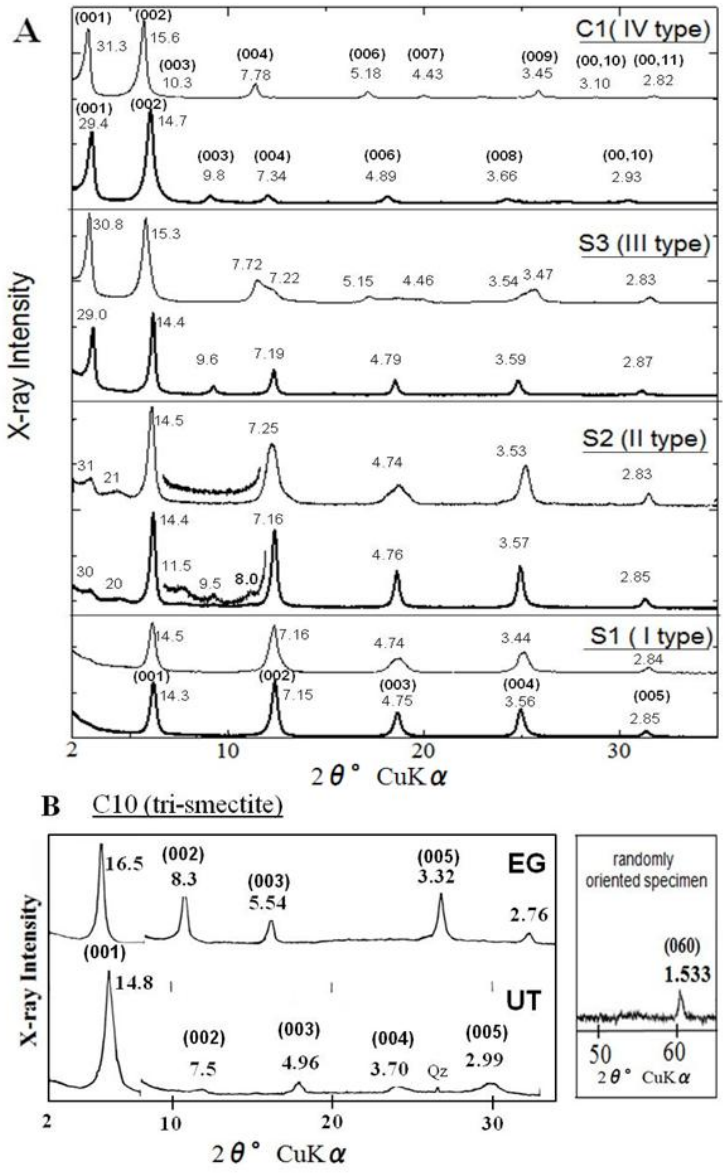

Fig. 6 XRD patterns of chlorite-corrensite-smectite series minerals of the selected ore samples (C1: #C50507, S1: #S80601, S2: #S72912, S3: #S80508B and C10: #C80304).

The d-spacings (Å) and indexes in parentheses are given near the XRD peaks (the same in the following illustrations). A: patterns (thick line: UT, thin line: EG) of chlorite-corrensite series minerals can be divided into four types (I–IV). Vertical lines are positions of basal reflections (14.2Å and its higher order reflections) corresponding to normal chlorite. B: Randomly oriented and oriented patterns of tri-octahedral smectite.

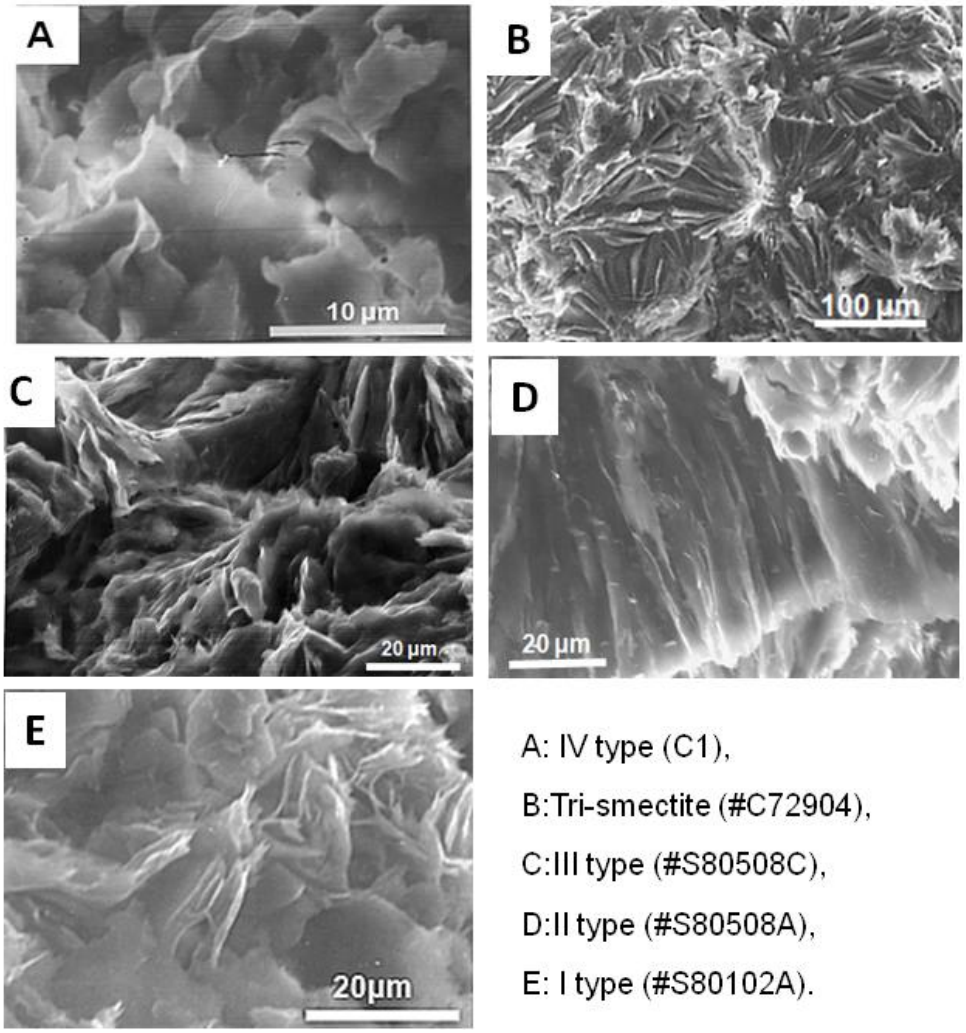

Fig. 7 Secondary electron images of chlorite-corrensite-smectite series minerals in selected samples.

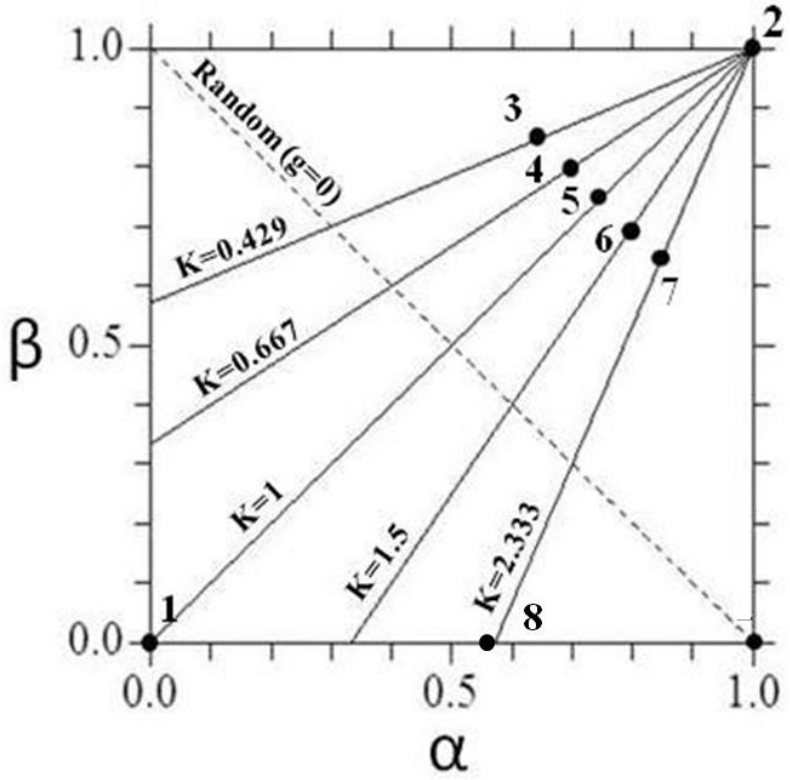

Fig. 8 Probability parameters used in this study for the calculations of the XRD patterns for the C/S interstratified structures. The location in the diagram is defined in terms of its own independent parameters of both existing layer probabilities (W_A and W_B) and transition probabilities (α and β). The relationship can be expressed as $\beta = K\alpha + (1-K)$ and $K = W_A/W_B$, where α is the probability from the layer A to the A and β is the probability from the layer B to the B. The points shown in numerals are used in this study. Points 1 and 8 are interstratifications (Reichweite g=1) respectively of regular and irregular type, points on the diagonal line (broken line) are random structure (Reichweite g=0), points from 3 to 7 are in the area of the segregation structure (the right above area to the diagonal dotted line), and point 2 is a completely segregated structure (Sato, 1965 & 1987).

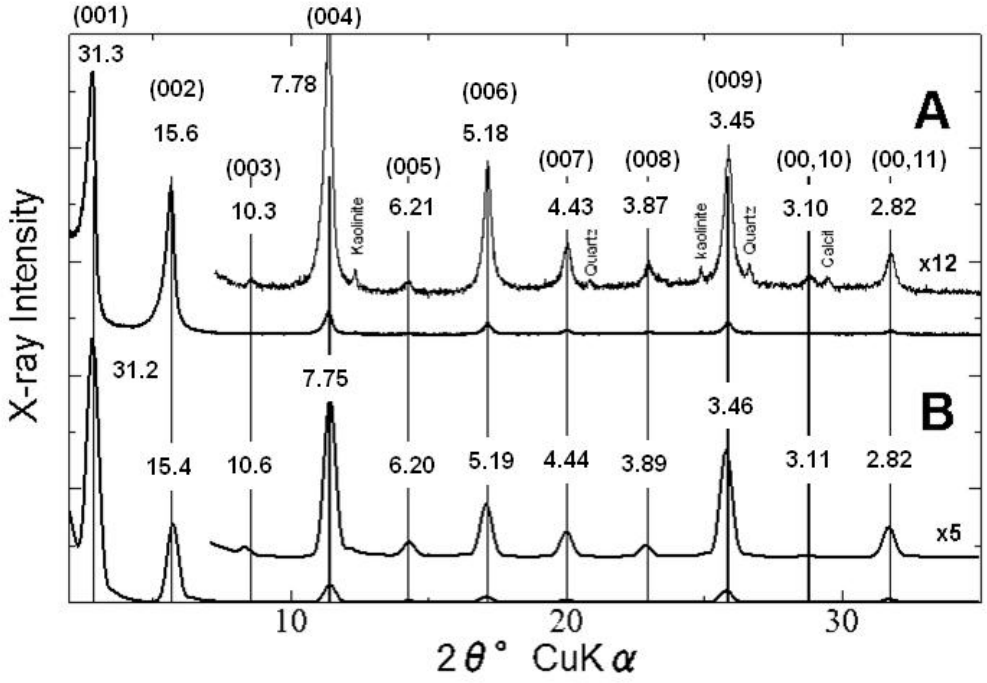

Fig. 9 (A) Observed XRD patterns of the EG-specimen (C1) of IV type, and (B) calculated XRD pattern of EG-corrensite, with probability parameters shown as point 1 (Reichweite g=1, regular interstratification) in Fig. 8. Vertical lines are corresponding to the basal reflections calculated for corrensite.

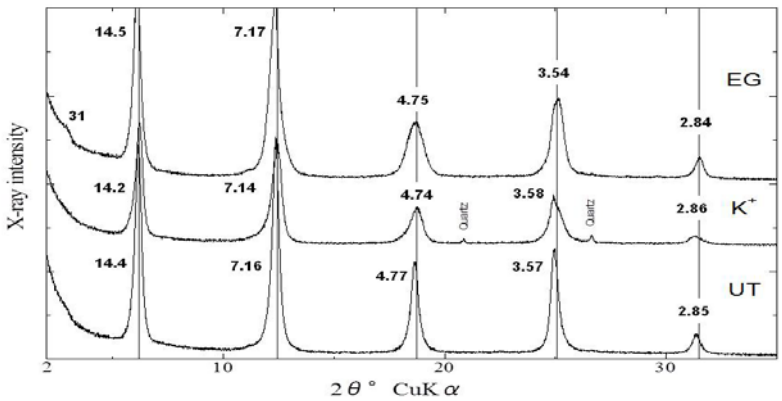

Fig. 10 Observed XRD patterns of EG-, K^+- and UT-specimens (S1: #S80601) of I type. Vertical lines are the positions of the basal reflections of chlorite.

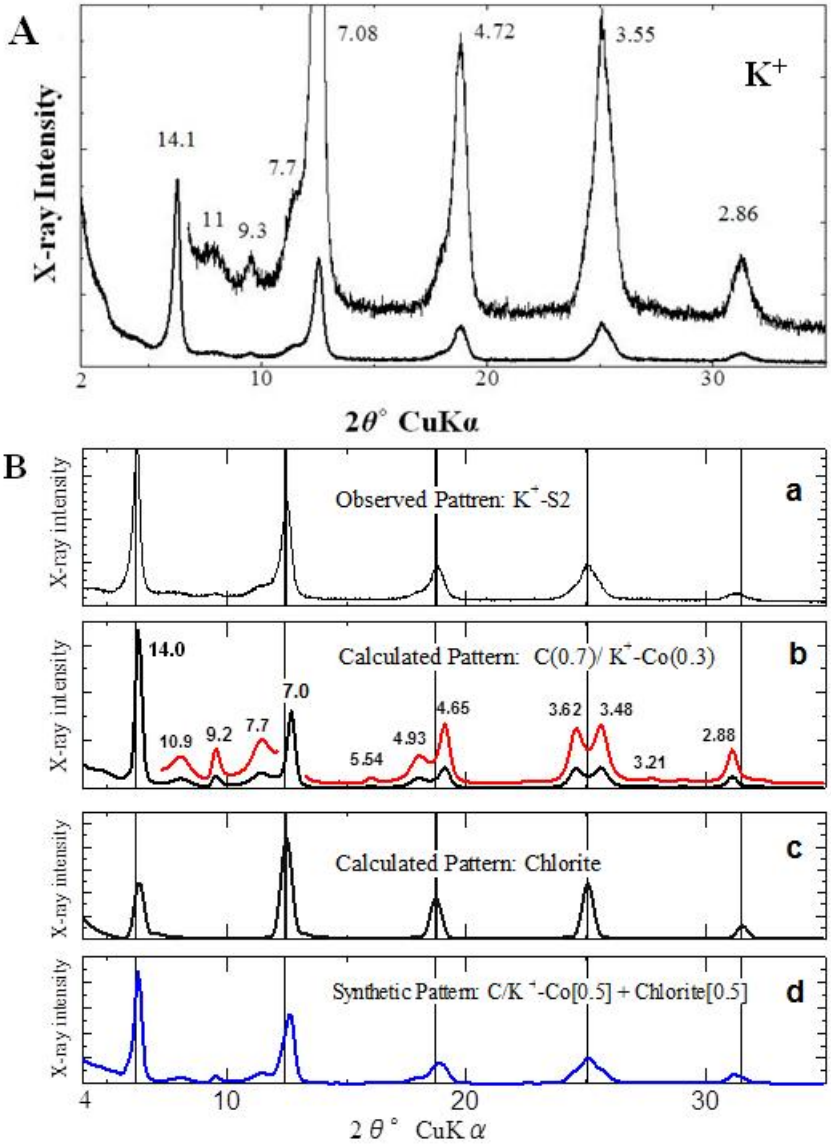

Fig. 11 (A) Observed XRD pattern of the K^+-specimens (S2) of the II type, and (B) a comparison between the observed pattern and the calculated patterns; a: observed pattern of the II type, b: calculated pattern of C/Co, c: calculated pattern of chlorite, d: synthetic pattern of C/Co and chlorite where the ratio can be estimated to be 0.5:0.5. Vertical lines are the positions of the basal reflections of chlorite.

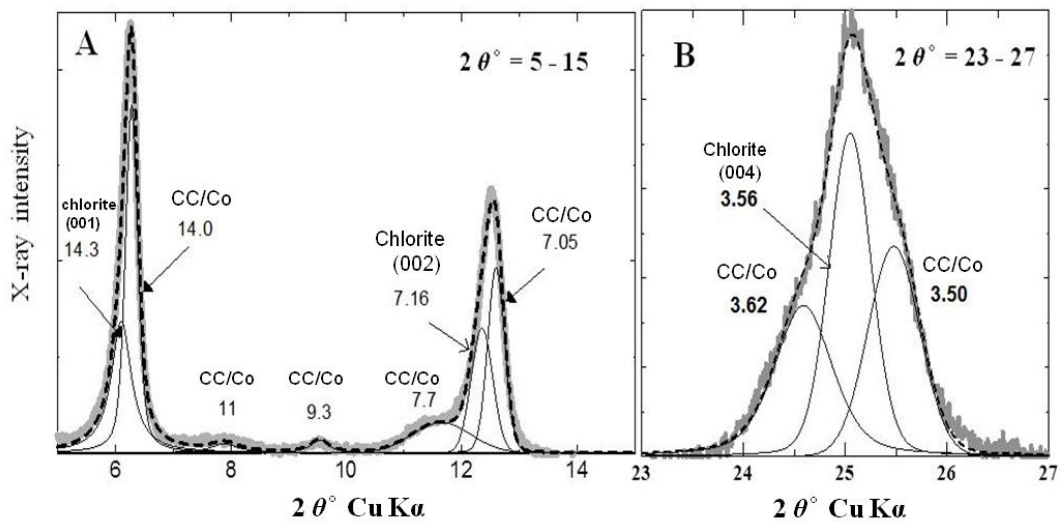

Fig. 12 XRD peak deconvolution for the observed pattern (K^+-specimen of sample S2) of II type. Thick gray curves are observed XRD patterns, and fine curves are decomposed peaks and broken curves are composed ones. Seven elementary peaks in (A) and three elementary peaks in (B) can be attributed to interstratified chlorite (0.7)/corrensite (0.3) mineral (14.0Å, 11 Å, 9.3 Å, 7.7 Å, 7.05 Å, 3.62 Å, and 3.50 Å), and to chlorite (14.3 Å, 7.16 Å, and 3.56 Å).

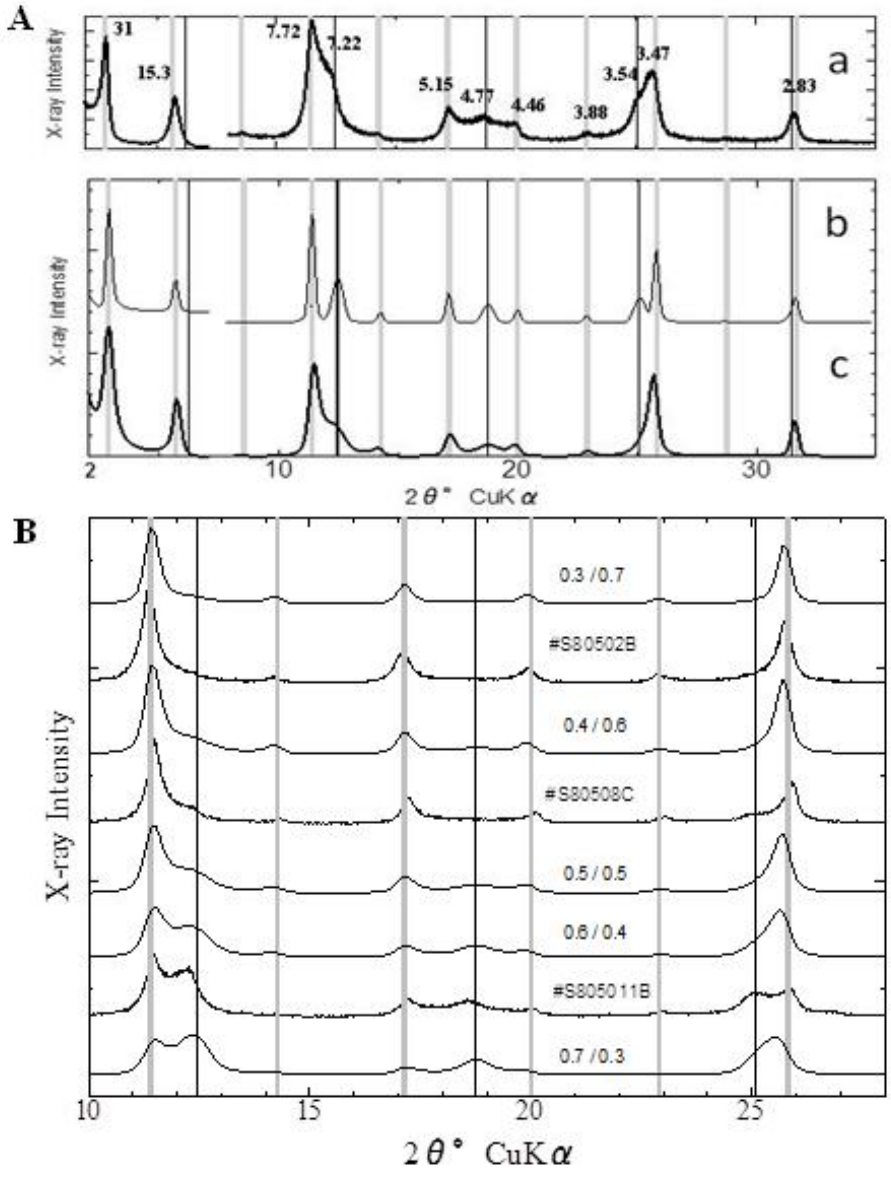

Fig. 13 (A) Observed XRD pattern of the EG-specimen (S3) of III type and calculated patterns of the discrete mixture and the segregation of chlorite and corrensite. Vertical fine and thick lines are the positions of the basal reflections of chlorite and calculated EG-corrensite, respectively. (B) Other EG-samples of the III type can be interpreted to be due to the C/S segregation structures with the ratios of the two layers between approximately 0.3(C)/0.7(Co) and 0.7(C)/0.3(Co).

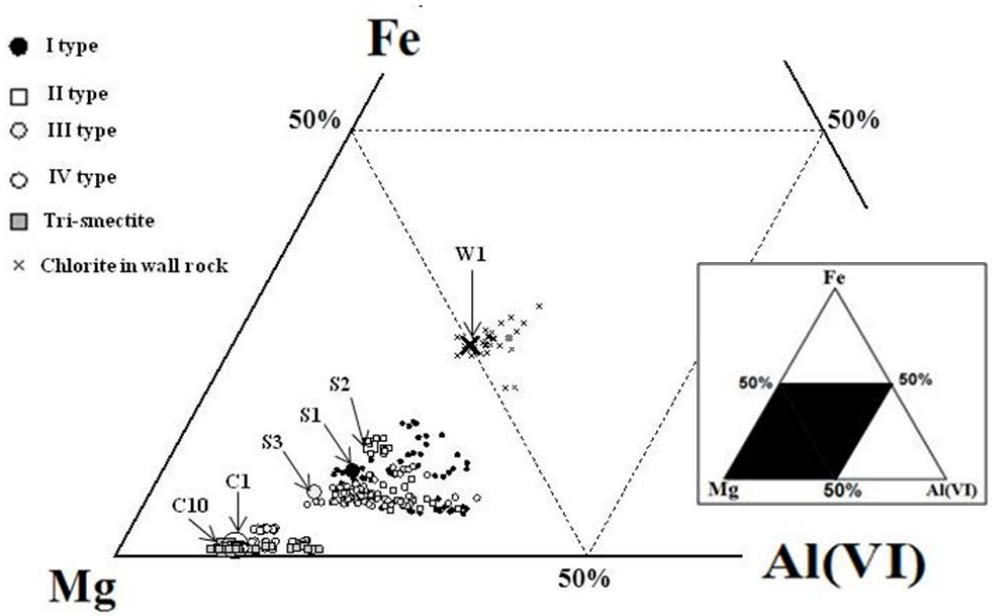

Fig. 14 Plot of Mg-Fe-Al^{VI} ratios of chlorite-corrensite-smectite series minerals from ore samples and chlorite from the wall rocks. 321 analyses (EPMA) are plotted. The Fe ratios increase in order from tri-smectite (0.1% ≥) and IV type (0.2% ≥) to III type (5−8%), II type (5−13%) and I type (4−15%) and to wall-rock chlorite (19−29%), and the Al (VI) ratios of the tri-smectite (9−20%) and IV type (9−18%) are plotted in a lower area on the diagram as compared with those of I, II and III types (16−31%, 17−31% and15−33%, respectively) and wall-rock chlorite (23−31%).

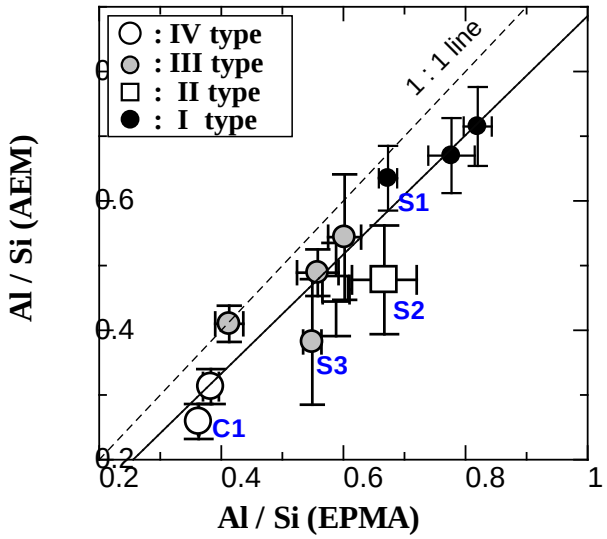

Fig. 15 Plot of analytical values of EPMA vs. AEM analyses for I–IV type minerals of selected ore samples.

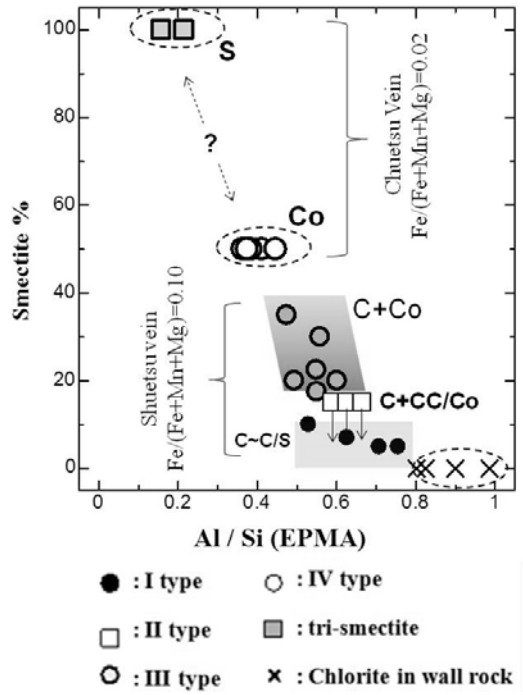

Fig. 16 Two mineralogical conversion series of chlorite-corrensite-smectite in the Todoroki epithermal ore veins: a corrensite-smectite series at the Chuetsu vein and a chlorite-corrensite series at the Shuetsu vein. Smectite % was estimated by the XRD modeling of C/S interstratification (see text).

TABLES

Table 1 Atomic parameters of the fundamental layers by reference to Reynolds (1980). Identical ratios of tetrahedral and octahedral compositions are used in all fundamental layers.

Chlorite (14.2 Å)

Atom	Z
1.75 Mg, 0.65 Fe, 0.6 Al	1.000
4 O, 2 OH	0.925
3.2 Si, 0.8 Al	0.806
6 O	0.770
6 OH	0.572
3.5 Mg, 1.3 Fe, 1.2 Al	0.500
6 OH	0.428
6 O	0.230
3.2 Si, 0.8 Al	0.194
4 O, 2 OH	0.075
1.75 Mg, 0.65 Fe, 0.6 Al	0.000

EG-Smectite (16.9 Å)

Atom	Z
1.75 Mg, 0.65 Fe, 0.6 Al	1.000
4 O, 2 OH	0.937
3.2 Si, 0.8 Al	0.837
6 O	0.807
1.7 CH_2O	0.638
1.7 CH_2O	0.582
1.2 H_2O	0.530
1.2 H_2O	0.470
1.7 CH_2O	0.418
1.7 CH_2O	0.362
6 O	0.194
3.2 Si, 0.8 Al	0.163
4 O, 2 OH	0.063
1.75 Mg, 0.65 Fe, 0.6 Al	0.000

Double layer chlorite (28.4 Å)

Atom	Z
1.75 Mg, 0.65 Fe, 0.6 Al	1.000
6 OH	0.964
6 O	0.865
3.2 Si, 0.8 Al	0.847
4 O, 2 OH	0.787
3.5 Mg, 1.3 Fe, 1.2 Al	0.750
4 O, 2 OH	0.713
3.2 Si, 0.8 Al	0.653
6 O	0.635
6 OH	0.536
3.5 Mg, 1.3 Fe, 1.2 Al	0.500
6 OH	0.464
6 O	0.365
3.2 Si, 0.8 Al	0.347
4 O, 2 OH	0.287
3.5 Mg, 1.3 Fe, 1.2 Al	0.250
4 O, 2 OH	0.213
3.2 Si, 0.8 Al	0.153
6 O,	0.135
6 OH	0.036
1.75 Mg, 0.65 Fe, 0.6 Al	0.000

K^+-corrensite (26.6 Å)

Atom	Z
1.75 Mg, 0.65 Fe, 0.6 Al	1.000
6 OH	0.962
6 O	0.856
3.2 Si, 0.8 Al	0.837
4 O, 2 OH	0.773
3.5 Mg, 1.3 Fe, 1.2 Al	0.733
4 O, 2 OH	0.693
3.2 Si, 0.8 Al	0.630
6 O	0.610
0.33 K, 2 H_2O	0.500
6 O	0.390
3.2 Si, 0.8 Al	0.370
4 O, 2 OH	0.307
3.5 Mg, 1.3 Fe, 1.2 Al	0.267
4 O, 2 OH	0.227
3.2 Si, 0.8 Al	0.164
6 O	0.144
6 OH	0.038
1.75 Mg, 0.65 Fe, 0.6 Al	0.000

EG-corrensite (31.1 Å)

Atom	Z
1.75 Mg, 0.65 Fe, 0.6 Al	1.000
6 OH	0.967
6 O	0.877
3.2 Si, 0.8 Al	0.860
4 O, 2 OH	0.806
3.5 Mg, 1.3 Fe, 1.2 Al	0.772
4 O, 2 OH	0.738
3.2 Si, 0.8 Al	0.683
6 O	0.667
1.7 CH_2O	0.575
1.7 CH_2O	0.544
1.2 H_2O	0.516
1.2 H_2O	0.484
1.7 CH_2O	0.456
1.7 CH_2O	0.425
6 O	0.333
3.2 Si, 0.8 Al	0.317
4 O, 2 OH	0.262
3.5 Mg, 1.3 Fe, 1.2 Al	0.228
4 O, 2 OH	0.194
3.2 Si, 0.8 Al	0.14
6 O	0.123
6 OH	0.033
1.75 Mg, 0.65 Fe, 0.6 Al	0.000

Table 2 Results of the EPMA analysis for the selected samples. Averaged oxide wt% (upper) and the structural formulae (lower) with standard deviations in parentheses are shown. N: the number of analyses.

Sample No.	S1	S2	S3	C1	C10	W1
	C-S minerals in ore samples					Chlorite
	I	II	III	IV	Smectite	
N	3	10	24	16	5	13
SiO_2	29.4	30.2(1.70)	34.8(0.73)	40.1(0.96)	48.1(0.78)	25.0(2.11)
TiO_2	0.0	0.0(0.01)	0.0(0.01)	0.0(0.01)	0.0(0.01)	0.0(0.01)
Al_2O_3	16.8	17.0(0.40)	16.2(0.31)	12.3(0.26)	6.5(0.31)	16.9(1.17)
FeO*	6.0	8.2(0.39)	4.5(0.28)	0.7(0.06)	0.3(0.02)	13.6(1.38)
MnO	6.3	3.6(0.62)	7.0(0.37)	4.2(0.50)	2.9(0.20)	2.3(0.20)
MgO	24.7	23.4(0.48)	25.5(0.69)	29.4(0.52)	20.4(0.57)	15.3(1.25)
CaO	0.2	0.3(0.06)	0.7(0.11)	1.3(0.20)	1.0(0.05)	0.2(0.05)
Na_2O	0.0	0.0(0.03)	0.0(0.02)	0.0(0.02)	0.1(0.06)	0.0(0.02)
K_2O	0.2	0.0(0.01)	0.0(0.01)	0.0(0.03)	0.1(0.03)	0.0(0.07)
Total	83.6	82.7	88.7	88.0	79.4	73.3
Si	6.05	6.23(0.22)	6.64(0.09)	6.63(0.08)	7.45(0.10)	6.01(0.13)
Al(IV)	1.95	1.77(0.22)	1.36(0.09)	1.37(0.08)	0.55(0.10)	1.99(0.13)
Al(VI)	2.12	2.38(0.07)	2.29(0.08)	1.03(0.07)	0.64(0.08)	2.83(0.10)
Fe	1.03	1.41(0.10)	0.72(0.05)	0.10(0.01)	0.04(0.00)	2.74(0.10)
Mn	1.10	0.62(0.10)	1.13(0.06)	0.57(0.09)	0.38(0.03)	0.46(0.05)
Mg	7.57	7.21(0.19)	7.24(0.13)	7.21(0.12)	4.71(0.14)	5.49(0.19)
Σ	11.82	11.62(0.12)	11.38(0.08)	8.93(0.08)	5.77(0.09)	11.53(0.09)
Ca	0.04	0.06(0.01)	0.15(0.02)	0.23(0.04)	0.16(0.01)	0.04(0.01)
Na	0.04	0.01(0.01)	0.01(0.01)	0.01(0.01)	0.03(0.02)	0.01(0.01)
K	0.06	0.00(0.00)	0.00(0.00)	0.01(0.01)	0.01(0.01)	0.01(0.02)
Base	$O_{20}(OH)_{16}$	$O_{20}(OH)_{16}$	$O_{20}(OH)_{16}$	$O_{20}(OH)_{10}$	$O_{20}(OH)_4$	$O_{20}(OH)_{16}$
Layer charge						
tetrahedral	-1.95	-1.77(0.22)	-1.36(0.09)	-1.37(0.08)	-0.55(0.10)	-1.99(0.13)
octahedral	1.79	1.63(0.20)	1.05(0.10)	0.90(0.11)	0.18(0.11)	1.89(0.15)
interlayer	0.18	0.14(0.03)	0.30(0.05)	0.47(0.07)	0.37(0.02)	0.09(0.03)
Al/Si	0.67	0.67(0.05)	0.55(0.02)	0.36(0.01)	0.16(0.01)	0.80(0.04)
Fe/(Fe+Mn+Mg)	0.11	0.15(0.01)	0.08(0.01)	0.01(0.00)	0.01(0.00)	0.32(0.01)

*FeO is expressed as total Fe.

Table 3 Results of the AEM analysis for the selected samples. Structural formulae based on averaged values with standard deviations in parentheses are shown. N: the number of analyzed particles.

Sample Name	S1	S2	S3	C1
Type	I	II	III	IV
N	7	15	19	8
Si	6.66(0.31)	7.00(0.53)	7.32(0.34)	7.88(0.23)
Al(IV)	1.34(0.31)	1.00(0.53)	0.68(0.34)	0.12(0.23)
Al(VI)	2.88(0.54)	2.30(0.33)	2.09(0.52)	1.92(0.17)
Fe	1.02(0.18)	1.83(0.24)	1.10(0.16)	0.15(0.04)
Mn	1.11(0.28)	0.51(0.08)	0.85(0.14)	0.36(0.08)
Mg	5.41(0.66)	6.15(0.81)	6.60(0.49)	5.47(0.28)
Ca	0.21(0.12)	0.06(0.08)	0.16(0.12)	0.11(0.09)
Na	1.06(0.69)	0.92(0.70)	0.89(0.78)	0.11(0.20)
K	0.13(0.12)	0.08(0.06)	0.11(0.11)	0.04(0.05)
Base	$O_{20}(OH)_{16}$	$O_{20}(OH)_{16}$	$O_{20}(OH)_{16}$	$O_{20}(OH)_{10}$
Al/Si	0.64(0.05)	0.48(0.08)	0.38(0.10)	0.26(0.03)
Fe/(Fe+Mn+Mg)	0.14(0.02)	0.22(0.03)	0.13(0.01)	0.04(0.02)

CAPTIONS

Fig. 1 Epithermal Au-Ag vein-type ore deposits where productions of interstratified C/S minerals have been described as vein minerals (Taguchi & Watanabe, 1973; Yoneda & Watanabe, 1981; Takeuchi, 1984; Yoneda & Watanabe, 1989).

Fig. 2 Geological map of the Todoroki Au-Ag ore deposits (Yoneda, 1994).

1: Talus deposit, 2: Tuff/sandstone with coal seam, 3: Andesitic tuff, 4: Sandstone/mudstone, 5: Rhyolitic tuff and tuff breccia, 6: Conglomerate/ mudstone/tuff, 7: Andesite lava, 8: Rhyolite, 9: Propylite, 10: Dolerite, 11: Fault, 12: Ore veins (C: Chuetsu vein, S: Shuetsu vein)

Fig. 3 Vein sketches showing the constituents and structures of the Chuetsu and Shuetsu veins. See in the text for details.

1: dark gray massive quartz (the I stage), 2: white/gray banded quartz with Au-Ag minerals/Cu-Pb-Zn-Fe-S sulfides (the II stage), 3: white/gray banded quartz with rhodochrosite and Au-Ag minerals/Cu-Pb-Zn-Fe sulfide minerals (the II stage), 4: gray quartz (partly banded) (the II stage), 5: white massive quartz (the II stage), 6: calcite (the III stage), 7: wall rock, 8: black streak rich in Au-Ag minerals/Cu-Pb-Zn-Fe sulfide minerals (AgB).

Fig. 4 Ore samples with ore minerals and clays from the middle stage quartz veins.

A: Banded quartz with Au-Ag minerals/Cu-Pb-Zn-Fe sulfide minerals (AgB) and clays (Chuetsau 130ml, #C80304), B: Banded quartz with rhodochrosite and clays (Chuetsau 50ml, #C71408), C: Banded quartz with AgB rich in Cu-Pb-Zn sulfides and clays crusting a rock fragment (Shuetsu central lower part, #S80509), D: quartz with patchy AgB and patchy ~ banded clays (Shuetsu eastern part, #S80601).

Fig. 5 Microphotographs of the clay minerals observed in the ore samples. A–C & E: transmitted light (cross polar), D: transmitted light (left half-parallel, right half-cross), F: reflected light (parallel polar). Bar scale: 100μm, Qz: quartz, CS: chlorite-smectite series mineral, Sm: smectite, Op: opaque ore mineral, Sp: sphalerite, El: electrum, Arg: argentite.

A: C1 (#C50507) − IV type, B: C10 (#C80304) − tri-smectite, C: #S80508C − III type, D: #S80508A − II type, E: #S80607 − I type, F: #C11204 − IV type. See in the text for details.

Fig. 6 XRD patterns of chlorite-corrensite-smectite series minerals of the selected ore samples (C1: #C50507, S1: #S80601, S2: #S72912, S3: #S80508B and C10: #C80304). The d-spacings (Å) and indexes in parentheses are given near the XRD peaks (the same in the following illustrations). A: patterns (thick line: UT, thin line: EG) of chlorite-corrensite series minerals can be divided into four types (I–IV). Vertical lines are positions of basal reflections (14.2Å and its higher order reflections) corresponding to normal chlorite. B: Randomly oriented and oriented patterns of tri-octahedral smectite.

Fig. 7 Secondary electron images of chlorite-corrensite-smectite series minerals in selected samples.

Fig. 8 Probability parameters used in this study for the calculations of the XRD patterns for the C/S interstratified structures. The location in the diagram is defined in terms of its own independent parameters of both existing layer probabilities (W_A and W_B) and transition probabilities (α and β). The relationship can be expressed as $\beta = K\alpha + (1 - K)$ and $K = W_A/W_B$, where α is the probability from the layer A to the A and β is the probability from the layer B to the B. The points shown in numerals are used in this study. Points 1 and 8 are interstratifications (Reichweite g=1) respectively of regular and irregular type, points on the diagonal line (broken line) are random structure (Reichweite g=0), points from 3 to 7 are in the area of the segregation structure (the right above area to the diagonal dotted line), and point 2 is a completely segregated structure (Sato, 1965 & 1987).

Fig. 9 (A) Observed XRD patterns of the EG-specimen (C1) of IV type, and (B) calculated XRD pattern of EG-corrensite, with probability parameters shown as point 1 (Reichweite g=1, regular interstratification) in Fig. 8. Vertical lines are corresponding to the basal reflections calculated for corrensite.

Fig. 10 Observed XRD patterns of EG-, K^+- and UT-specimens (S1: #S80601) of I type. Vertical lines are the positions of the basal reflections of chlorite.

Fig. 11 (A) Observed XRD pattern of the K^+-specimens (S2) of the II type, and (B) a comparison between the observed pattern and the calculated patterns; a: observed pattern of the II type, b: calculated pattern of C/Co, c: calculated pattern of chlorite, d: synthetic pattern of C/Co and chlorite where the ratio can be estimated to be 0.5:0.5. Vertical lines are the positions of the basal reflections of chlorite.

Fig. 12 XRD peak deconvolution for the observed pattern (K^+-specimen of sample S2) of II type. Thick gray curves are observed XRD patterns, and fine curves are decomposed peaks and broken curves are composed ones. Seven elementary peaks in (A) and three elementary peaks in (B) can be attributed to interstratified chlorite (0.7)/corrensite (0.3) mineral (14.0Å, 11 Å, 9.3 Å, 7.7 Å, 7.05 Å, 3.62 Å, and 3.50 Å), and to chlorite (14.3 Å, 7.16 Å, and 3.56 Å).

Fig. 13 (A) Observed XRD pattern of the EG-specimen (S3) of III type and calculated patterns of the discrete mixture and the segregation of chlorite and corrensite. Vertical fine and thick lines are the positions of the basal reflections of chlorite and calculated EG-corrensite, respectively. (B) Other EG-samples of the III type can be interpreted to be due to the C/S segregation structures with the ratios of the two layers between approximately 0.3(C)/0.7(Co) and 0.7(C)/0.3(Co).

Fig. 14 Plot of Mg-Fe-Al^{VI} ratios of chlorite-corrensite-smectite series minerals from ore samples and chlorite from the wall rocks. 321 analyses (EPMA) are plotted. The Fe ratios increase in order from tri-smectite (0.1% ≥) and IV type (0.2% ≥) to III type (5−8%), II type (5−13%) and I type (4−15%) and to wall-rock chlorite (19−29%), and the Al (VI) ratios of the tri-smectite (9−20%) and IV type (9−18%) are plotted in a lower area on the diagram as compared with those of I, II and III types (16−31%, 17−31% and15−33%, respectively) and wall-rock chlorite (23−31%).

Fig. 15 Plot of analytical values of EPMA vs. AEM analyses for I–IV type minerals of the selected ore samples.

Fig. 16 Two mineralogical conversion series of chlorite-corrensite-smectite in the Todoroki epithermal ore veins: a corrensite-smectite series at the Chuetsu vein and a chlorite-corrensite series at the Shuetsu vein. Smectite % was estimated by the XRD modeling of C/S interstratification (see text).

Table 1 Atomic parameters of the fundamental layers by reference to Reynolds (1980). Identical ratios of tetrahedral and octahedral compositions are used in all fundamental layers.

Table 2 Result of the EPMA analysis for selected samples. Averaged oxide wt% (upper) and the structural formulae (lower) with standard deviations in parentheses are shown. N: the number of analyses.

Table 3 Result of the AEM analysis for selected samples. Structural formulae based on averaged values with standard deviations in parentheses are shown. N: the number of analyzed particles.